Title: Efficacy and micro-characterization of pathophysiological events on caries-affected dentin treated with glass-ionomer cements.

Authors: Manuel Toledano[1*], Fátima S. Aguilera[1], Estrella Osorio[1], Inmaculada Cabello[1], Manuel Toledano-Osorio[1], Raquel Osorio[1].

Institution: [1]University of Granada, Faculty of Dentistry, Dental Materials Section.

Address: [1]University of Granada, Faculty of Dentistry, Dental Materials Section

Colegio Máximo de Cartuja s/n

18071 – Granada - Spain.

*Corresponding author: Prof. Manuel Toledano

University of Granada, Faculty of Dentistry

Dental Materials Section

Colegio Máximo de Cartuja s/n

18071 – Granada - Spain.

Tel.: +34-958243788

Fax: +34-958240809

Email: toledano@ugr.es

ABSTRACT

The aim of this study was to evaluate if mechanical cycling influences bioactivity and bond strength at the glass-ionomer cement-dentin interface, after load cycling. Microtensile bond strength (MTBS) was assessed with Ketac-Bond (conventional glass ionomer/GIC) or Vitrebond Plus (resin-modified/RMGIC), in sound dentin or in caries-affected dentin (CAD). Debonded dentin surfaces were studied by field emission scanning electron microscopy (FESEM), and remineralization was evaluated through nanohardness (Hi) and Young's modulus (Ei), Raman spectroscopy, and Masson's trichrome staining technique. Load cycling did not affect MTBS, except when Ketac-Bond was applied on sound dentin, which attained 100% pretesting failures. Minerals precipitated in porous platforms. GIC promoted total occlusion of tubules, and RMGIC originated empty or partial occluded tubules. In sound dentin, load cycling produced an increase of the relative presence of crystalline minerals after using Ketac-Bond (Phosphate peak, from 18.04 up to 81.29 cm^{-1} at hybrid layer, and from 19.28 up to 108.48 cm^{-1} at the bottom of the hybrid layer; Carbonate peak, from 8.06 up to 15.43 cm^{-1} at the hybrid layer, and from 7.22 up to 19.07 cm^{-1} at the bottom of the hybrid layer). Vitrebond Plus, in sound dentin, attained opposite outcomes. In CAD treated with Ketac- Bond, the highest Hi (1.11 GPa) and Ei (32.91 GPa) values were obtained at the hybrid layer after load cycling. This GIC showed increased and immature mineral components (an average of 25.82 up to 30.55 cm^{-1}), higher frequencies of crosslinking (considering the pyridinium ring at hybrid layer, from 4.1 up to 6.86 cm^{-1}; at bottom of the hybrid layer, from 7.55 up to 8.58 cm^{-1}) and worst collagen quality (considering the ratio amide I/AGEs-pentosidine at the hybrid layer, from 0.89 up to 0.69 cm^{-1}; at the bottom of the hybrid layer, from 1.39 up to 1.29 cm^{-1}) after load cycling, at the interface of the CAD samples. Both Hi and Ei of CAD treated with RMGIC were not affected

after load cycling, though phosphates, carbonates and crystallinity increased. The organic components showed a dissimilar crosslinking and an improvement of the nature of collagen. Trichrome staining showed lower signs of demineralization or exposed proteins after mechanical loading, though Vitrebond Plus exhibited a slight increment in red intensity at the interface. The null hypothesis to be tested is that bond strength, chemical bonding and mechanical performance of the tested ionomer-based cements would not be influenced by the application of load cycling on restorations of sound and caries-affected dentin substrates.

1. Introduction

Sound dentin is mainly composed of type I collagen fibrils with associated noncollagenous proteins, forming a three-dimensional matrix that is reinforced by mineral [1], but non carious dentin is not the substrate most frequently involved in clinical dentistry. Instead, dentists usually must bond adhesive materials to irregular dentin substrates such as carious dentin [2]. Caries-affected dentin (CAD) is partially demineralized and more porous than noncarious dentin with a predominantly intact collagen matrix, whose collagen fibrils retain their banded structure and intermolecular crosslinks [3]. It should be preserved during clinical treatment because it is remineralizable and serves as a suitable substrate for dentin adhesion [4] and physiologic remineralization [5]. Adhesive materials such as glass ionomer cements (GICs) have been clinically proposed for this aim; their potential for chemical interactions with both resin and water-based cement-like materials have been stated [5]. One of the more interesting uses of GICs has been the atraumatic restorative technique for stabilization of caries lesions in countries where routine dental care is not available [6].

Conventional GIC is formed of fluoro-aluminosilicate glass (powder) and an aqueous solution of polyalkenoic acid, such as polyacrylic acid (liquid). Upon mixing, an acid-base reaction takes place between the polyalkenoic acid and the ion-leachable glass particles. During the dissolution phase, ions such as aluminium, fluoride, calcium and strontium are released. Cross linking between polyacid's carboxylic groups and ions are facilitated in the latest stage of gelation [5,7]. GICs are characterized by their self-adhesiveness, claimed to depend upon chemical interaction of polyalkenoic acids with inorganic tooth constituents [8]. Previous application of a respective conditioner is mandatory, in order to remove the smear layer and partially demineralize the dentin

substrate, with exposure of a micro-porous collagen fibrils network in which hydroxyapatite crystals remains attached [9]. Consequently, formation of a shallow hybrid layers (~1-2 μm depth) [10,11] definitely contribute to micro and nano-mechanical bonding, as with resin-based adhesives [12, 13]. The most important disadvantages of conventional GICs are poor performance as a restorative material particularly regarding esthetics, the lack of sufficient strength, toughness and wear resistance, decrease setting time, and attenuate moisture sensitivity. To offset this drawback, resin-modified glass-ionomers (RMGIs) have been introduced [13].

Resin-modified glass-ionomer cements (RMGICs) are typically powder/liquid formulations which set, when mixed, through an acid-base reaction between ion-leachable glasses and polyalkenoic acids, as well as upon light-polymerization of water-soluble (metha)crylate, such as HEMA and photoinitiators [14]. In both GICs and RMGICs, aluminium, fluoride and calcium or strontium leach out of the cement as the glass is being dissolved by the polyacid, while calcium and phosphate ions also move out of the underlying dentin as a result of the self-etching effect of the setting cement on mineralized dentin [15]. Chemical interaction is the primary bonding mechanism for RMGICs, in addition to micro-mechanical interlocking into surface irregularities [16], hybridizing dentin. When RMGICs are applied without separate conditioners, micro-mechanical bonding is limited to retention provided by the intrinsic surface roughness of dentin, and porosity created by the RMGIC self-etching characteristics [9]. Hypomineralized and porous CAD substrate may allow deeper penetration of the acidic compounds, leading to a deeper demineralization with diffused monomer [2], creating a much thicker hybrid layer (HL) over a zone of non infiltrated but demineralized collagen substratum, the bottom of the hybrid layer (BHL). This unprotected collagen may become the sites for collagen hydrolysis by host-derived matrix metalloproteinases

(MMPs) enzymes [17], and it deserves attention to know if the adhesive material occupies all the space left by the mineral after conditioning [18].

The longevity of adhesive restorations and its clinical success are influenced by the mechanical and chemical properties of the materials and by the restorative technique, which directly affect hybrid layer quality and bond strength [19,20]. In the oral environment, teeth are subjected to challenges provided by mechanical stresses from mastication and para-functional habits. Mechanical cycling has been widely used as potential aging methods that, additionally, stimulate challenges *in vitro*, *i.e.*, dentin remineralization [21]. Remineralization is the process of delivery of mineral (calcium and phosphate), from outside the tooth into previously demineralized hard tissue. Fluoride, calcium and phosphate are the three major ions for tooth remineralization [22]. Additionally, the application of GIC to a caries lesion induces a reduction in lesion depth. This may be due not only to the fluoride-releasing but to the recharging ability of GICs. Fluoride can be taken up into the cement from the oral cavity and released again. Similarly, GIC could act as a fluoride reservoir [23].

There exists scarce information on the nature of the dentin-restorative (GIC/RMGIC) interactions, since the subnanostructural characteristics of those interfaces have not been investigated to any great extent. This study used microtensile bond strength (MTBS), field-emission SEM (FESEM), nanohardness and Young's modulus (Hi, Ei), Raman analysis, and Masson's trichrome staining to examine the regional differences in the ultra-structure of both a GIC and a RMGIC onto sound and caries-effected dentin substrata. Thereby, this investigation assessed the bond strength, chemical interaction and mechanical performance of sound and caries-affected dentin surfaces treated with both a conventional glass-ionomer and a resin-modified glass-ionomer cement, submitted or not to mechanical loading. The null hypothesis to be

tested is that bond strength, chemical bonding and mechanical performance of the tested ionomer-based cements would not be influenced by the application of load cycling on restorations of sound and caries-affected dentin substrates.

2. Material and Methods

2.1. Specimen preparation, bonding procedures and mechanical loading

Eighty human third molars (forty sound specimens and forty with occlusal caries) were obtained with informed consent from donors (20–40 year of age), under a protocol approved by the Institution Review Board. Molars were stored at 4ºC in 0.5% chloramine T for up to 1 month before use. A flat mid-coronal sound or carious dentin surface was exposed using a hard tissue microtome (Accutom-50; Struers, Copenhagem, Denmark) equipped with a slow-speed, water-cooled diamond wafering saw (330-CA RS-70300, Struers, Copenhagen, Denmark). The inclusion criteria for carious teeth were that the caries lesion, surrounded by sound dentin, should be limited to the occlusal surface, that it extended at least half the distance from the enamel-dentin junction to the pulp chamber. To obtain caries-affected dentin, grinding was performed by using the combined criteria of visual examination, surface hardness using a dental explorer, and staining by a caries detector solution (CDS, Kuraray Co., Ltd., Osaka, Japan). Using this procedure it was removed all soft, stainable, carious dentin. It was left the relatively hard, caries-affected non staining dentin, on the experimental side. A 180-grit silicon carbide (SiC) abrasive paper mounted on a water-cooled polishing machine (LaboPol-4, Struers, Copenhagem, Denmark) was used to produce a clinically relevant smear layer [24]. A conventional glass ionomer cement, Ketac-Bond (3M Deustchland GmbH, Neuss, Germany) and a resin-modified glass ionomer cement, Vitrebond Plus (3M Deustchland GmbH, Neuss, Germany) were tested. The chemical components and descriptions of the materials are provided in Table 1. Glass ionomer

cements were applied in sound or caries-affected dentin following the manufacturer´s instructions, and a flowable resin composite (X-FlowTM, Dentsply, Caulk, UK) was placed incrementally in five 1 mm layers and light-cured with a Translux EC halogen unit (Kulzer GmbH, Bereich Dental, Wehrheim, Germany) for 40 s. Half of the carious teeth were stored for 24 h in simulated body fluid solution (SBF) (ISO 23317 method), and the other half were submitted to mechanical loading, in SBF (100,000 cycles, 3 Hz, 49 N) (S-MMT-250NB; Shimadzu, Tokyo, Japan) [25]. The load cycling lasted for 9 hours and 15 minutes; the rest of the time until complete 24 h, the loaded specimens were kept in SBF, at 37 ºC. Diagram 1 shows how samples were prepared for testing.

2.2. Microtensile Bond Strength

After the different procedures, 48 teeth (six from each group) were sectioned into serial slabs, perpendicular to the bonded interface to produce bonded sections of approximately 1.0 mm thick. This yielded about three slabs of bonded sound or caries-affected dentin, *per* tooth. Eighteen slabs from each experimental group were used for bond strength evaluation. Slabs were hand trimmed with a fine diamond bur into hourglass-shaped specimens, with the smallest dimension at the bonded interface (1mm^2). This trimming technique was chosen in order to accurately delimit the bonded tissue of interest (caries-affected dentin). Similar procedure was followed in the group of sound dentin, in order to reproduce analogous methodology. Specimens were attached to a modified Bencor Multi-T testing apparatus (Danville Engineering Co., Danville, CA) with a cyanoacrylate adhesive (Zapit/Dental Venture of America Inc., Corona, CA, USA) and stressed to failure in tension (Instron 4411 /Instron Inc., Canton, MA, USA) at a crosshead speed of 0.5 mm/min. The cross-sectional area at the site of failure of the fractured specimens was measured to the nearest 0.01mm with a pair of

digital calipers (Sylvac Ultra-Call III, Fowler Co Inc., Newton, Mass, USA). Bond strength values were calculated in MPa.

Fractured specimens were examined with a stereomicroscope (Olympus SZ-CTV, Olympus, Tokyo, Japan) at 40x magnification to determine the mode of failure. Failure modes were classified as adhesive or mixed. Representative specimens of each group were fixed in a solution of 2.5% glutaraldehyde in 0.1 mol/L sodium cacodylate buffer for 24 h, rinsed three times in 0.1 mol/L sodium cacodylate buffer. Samples were placed in an apparatus for critical point drying (Leica EM CPD 300, Wien, Austria). They were then sputter-coated with carbon by means of a sputter-coating Nanotech Polaron-SEMPREP2 (Polaron Equipment Ltd., Watford, UK) and observed with a field emission scanning electron microscope (FESEM Gemini, Carl Zeiss, Oberkochen, Germany) at an accelerating voltage of 3 kV. Energy-dispersive analysis was performed in selected points using an X-ray detector system (EDX Inca 300, Oxford Instruments, Oxford, UK) attached to the FESEM. MTBS values were analyzed by two-way ANOVA (independent factors are mechanical loading and cement type) and Student Newman Keuls multiple comparisons tests. For all tests, statistical significance was set at a = 0.05.

2.3. Measurement of nanohardness and Young's modulus

Sixteen molars were used for the test. An atomic force microscope (AFM-Nanoscope V, Digital Instruments, Veeco Metrology group, Santa Barbara, CA, USA) equipped with a Triboscope indentor system (Hysitron Inc., Minneapolis, MN, USA) and a Berkovich indenter (tip radius 20 nm) was employed for the indentation process in a fully hydrated status [26]. For each subgroup, three slabs were tested. On each slab, five indentation lines were executed in five different mesio-distal positions along the interface in a straight line starting from the adhesive layer down to the intertubular

dentin. Indentations were performed with a load of 4000 nN and a time function of 10 s. The distance between each indentation was kept constant by adjusting the distance intervals in 5 (±1) μm steps [27]. Hardness (Hi) and modulus of elasticity (Ei) data were registered in GPa. Data were analyzed by two-way ANOVA (independent factors were mechanical loading and adhesive procedure) and Student–Newman–Keuls multiple comparisons ($P < 0.05$).

2.4. *Raman spectroscopy and cluster analysis*

A dispersive Raman spectrometer/microscope (Horiba Scientific Xplora, Villeneuve d′Ascq, France) was also used to analyze bonded interfaces. A 785-nm diode laser through a X100/0.90 NA air objective was employed. Raman signal was acquired using a 600-lines/mm grafting centered between 900 and 1,800 cm^{-1}. Chemical mapping of the interfaces were performed. For each specimen two 25μm x 25μm areas of the interfaces at different sites were mapped using 1.8 μm spacing at X axis and 1 μm at Y axis. Chemical mapping was submitted to K-means cluster (KMC) analysis using the multivariate analysis tool (ISys® Horiba), which includes statistical pattern to derive the independent clusters. Hypotheses concerning the number of clusters formed in resin-bonded interfaces were previously obtained [28]. However, Ward's method was employed to get some sense of the number of clusters and the way they merge from the dendrogram. The aim of a factor analysis lies in the effective reduction of the dataset dimension while maintaining a maximum of information. This method was used to model the data and to determine spectral variances associated for data differentiation. It resulted in the calculation of a new coordinate system whereby variations of the dataset is described via new axes, principal components (PCs). The K-means clustering is a method of analysis based on a centroid model which aims to partition n observations into k clusters in which each observation belongs to the cluster with the nearest mean

[29]. The natural groups of components (or *data*) based on some similarity and the centroids of a group of *data* sets were found by the clustering algorithm once calculated by the software. To determine cluster membership, this algorithm evaluated the distance between a point and the cluster centroids. The output from a clustering algorithm was basically a statistical description of the cluster centroids with the number of components in each cluster. The biochemical content of each cluster was analyzed using the average cluster spectra. Four clusters were identified and values for each cluster such as adhesive (ADH), absortion layer (AL), hybrid layer (HL), and dentin (DEN), within the interface, were independently obtained. Principal component analysis (PCA) decomposed *data* set into a bilinear model of linear independent variables, the so-called principal components (PCs). The observed spectra were described at 900-1800 cm^{-1} with 10 complete overlapping Gaussian lines, suggesting homogeneous data for further calculations [30, 31]. As the cluster centroids are essentially means of the cluster score for the elements of cluster, the mineral, organic and adhesive components of interfaces were examined for each cluster. A comparison of the spectra that were collected from the three specimens which compose each subgroup indicated complete overlap, suggesting similarity between both measurements. At this point, the mineral and organic component of dentin, and the degree of the adhesive presence, at the resin-dentin interface were analyzed as follows [32]:

Relative presence of mineral:

1. *Phosphate* (960 cm^{-1}) *and carbonate* (1070 cm^{-1}) *peaks and areas of their bands.* Peak heights were processed in absorbance units.

2. *Relative mineral concentration* (RMC) (*i.e.,* mineral-to-matrix ratio): It was inferred from the visible ratio of the intensities of the peaks at 960 cm^{-1} (phosphate) (PO_4^{3-}) and 1003 cm^{-1} (phenyl group), the aromatic ring of

phenylalanine residues in collagen. These indexes concerned with the maximum relative degree of mineralization [33,34]. Additionally, peaks at 960 cm^{-1} and 1450 (CH$_2$) or 1070 cm^{-1} and 1450 can be used [35].

Crystallinity: It was evaluated based on the full width at half maximum (FWHM) of the phosphate band at 960 cm^{-1} and carbonate band at 1070 cm^{-1}. These indexes expressed the crystallographic or relative atomic order, since narrower peaks suggest less structural variation in bond distances and angles [33]. In general, the narrower the spectral peak width is, the higher the degree of mineral crystallinity [34].

Gradient in mineral content (GMC), or carbonate content of the mineral crystallites: It was assessed as the relationship between the ratio of heights at 1070 cm^{-1} (carbonate) (CO$_3^{2-}$) to 960 cm^{-1} (phosphate) (PO$_4^{3-}$), indicating carbonate substitution for phosphate [33].

Phosphate peaks ratio (PPR/mPPR): it assesses the ratio between the mineral peak at 960 cm^{-1} (phosphate) (PO$_4^{3-}$), within the demineralized zone and the mineral peak (PO$_4^{3-}$) within the healthy substratum (PPR) [36] or caries-affected substratum (mPPR) [32].

Chemical acids and their salts, at 1262 cm^{-1}: this peak corresponds to the overlapping of smaller peaks that represent the polyacrylic and tartaric acids and their salts [37].

The organic component of dentin was analyzed examining the following parameters:

Normalization: Phenyl group: The peak at 1003 cm^{-1}, which is assigned to C-C bond in the phenyl group, was used for normalization [38].

Crosslinking:

1. Pyridinium ring vibration: In the spectra, the peak appeared at 1030/1032.7 cm^{-1}, is assigned to the C-C in pyridinium ring vibration which has a trivalent amino

acid crosslinking residue [39]. The relative intensity of this peak increases after the crosslinking formation [40].

2. Ratio Pyridinium/Phenyl (1032 cm^{-1}/1001 cm^{-1}): the higher the ratio, the greater the extend of collagen cross-linking [40,41].

3. Ratio 1003 (phenyl)/1450 (CH$_2$): arises preceding deposition of HAP (hydroxyapatite) crystals within the structure [35].

4. AGEs (advance glycation end products)-pentosidine at 1550 cm^{-1}, interpreted as a marker of the aging process [42].

Nature of collagen:

1. Amide III, CH$_2$ and amide I: The peaks at 1246/1270, 1450 and 1655/1667 cm^{-1}, assigned to amide III, CH$_2$ and amide I, respectively, are sensitive to the molecular conformation of the polypeptide chains [38,40]. The decrease of amide I peak indicates damage or removal of collagen fibrils [38].

2. Ratio amide I/amide III concerned the organization of collagen.

3. Ratio amide III /CH$_2$ wagging mode indicates the structural differences [43].

4. Ratio amide I/CH$_2$ indicates altered collagen quality [43].

5. Ratios amide III and I/AGEs-Pentosidine, indicatives of the glycation reaction *vs* collagen scaffolding [43].

6. 1340 cm^{-1} peak: This signal has been assigned to protein α-helices where intensity is sensitive to molecular orientation [35].

Carboxilic group COO$^-$: The 1415 cm^{-1} band assigned to COO$^-$ stretching mode is related with the formation of ionic bonds with calcium [44].

Lipids: Detection of extra-cellular lipids and phospholipids bands at 1440 and 1465 cm^{-1} reveals the presence of debris of cell membranes, and play an important role during the early stage of hard tissue healing or maturation [45].

2.5. *Light microscopy–Masson's trichrome staining*

Two resin-dentin bonded slices of each group were used for the histo-morphological evaluations. Each slice was fixed in a glass holder with a photo curing adhesive (Technovit 7210 VLC, Heraeus KulzerGmbH Co., Werheim, Germany) and ground with SiC papers of increasing fine grits (800, 1000, 1200 and 4000) in a polisher (Exakt, Apparatebau D-2000, Norderstedt, Germany) until its thickness was approximately 10 mm. Slices were stained with Masson's trichrome for differentiation of resin and non-resin encapsulation of the exposed collagen. This dye has a high affinity for cationic elements of normally mineralized type I collagen, resulting in staining collagen green, and when demineralized, resulting in different coloration, generally red; collagen coated with adhesive stains orange and pure adhesive appears beige. Slices with adherent stained sections were dehydrated through ascending ethanol and xylene. The sections were cover slipped and examined by light microscopy (BH-2, Olympus, Tokyo, Japan) at 100× magnifications. Three slices were prepared from each specimen, and images were digitalized in a scanner (Agfa Twin 1200, Agfa-Gevaert NV Mortsel, Belgium). In each specimen, the presence or absence of a red band (that would correspond to demineralized dentin) was observed. A qualitative assessment of the collagen encapsulation was completed by observing color differences within the interfacial zones of resin-dentin interfaces [46].

3. Results and discussion

Attained microtensile bond strength (mean and standard deviation), and nanomechanical properties (mean and standard deviation), for each group are displayed in Figures 1, 2-3, respectively. Raman analysis is represented in Figure 4. Light micrographs interfaces stained with Masson's trichrome are shown in Figure 5. FESEM and EDX analysis is displayed in Figures 6 and 7.

Our results confirm that load cycling of caries-affected dentin surfaces treated with Ketac Bond (GIC) and Vitrebond Plus (RMGIC) promote an increase of mineralization at the cement-dentin interface. In GIC, mineral growing became associated to higher frequencies of crosslinking and better mechanical performance, as crystals preferentially nucleated at intrafibrillar compartment, giving rise to a bigger advance of mineral precipitation in comparison with RMGIC.

The adhesive potential and remineralization capability of two ionomer-based cements applied on sound and CAD substrata have been investigated. The null hypothesis was partially accepted, as mechanical loading did not influence bond strength results, as all unloaded and load cycled samples performed similar (Fig. 1A). The formation of strong ionic bonds between polyalkenoic acid, which provides the acidic functional groups, and calcium may have contributed to the higher attained stability of bond strength values [16], regardless of load cycling application. These findings are in agreement with other studies that observed relatively low bond strength of GICs [20]. The lowest percentage of adhesive failures was achieved after mechanical loading (Fig. 1B). Strengthened of the cement-dentin interface from remineralization may have accounted for this outcome as, observing FESEM analysis, multiple mineral precipitates were encountered deposited and integrated at the interface and within some tubules, which appeared totally or partially mineral-filled. After debonding and fractographic analysis, sound and caries-affected dentin surfaces treated with Vitrebond Plus (RMGIC) showed an increase in the percentage of mixed failures after load cycling (Fig. 1B). The rather superficial mechanical interlocking might be responsible for this, possibly associated to the lack of a previous conditioning step [13]. Those dentin surfaces disclosed new mineral cumuli on both peritubular and intertubular dentin (Figs. 6C, 7C), and multiple rods-like formations at the interface in the load cycled groups

(Figs. 6D, 7D). In the unloaded specimens treated with Vitrebond Plus, elemental analysis (Fig. 6C-EDX) showed P and Ca as main components, but lower fractions of Al, Na and Sr were also detected, which became integrated in this porous, non-particulate, poly(HEMA)-rich hydrogel layer [47], the absorption layer [23]. This 7-10 µm thick structure [10] was first reported by Watson and Barlett (1994) [48] , and contains some of the ions released by the initial acid-base glass-ionomer reaction between the fluoro-aluminosilicate glass particles, hydroxyapatite and polyacids and is crucial for mediating the bond between RMGICs and dentin [10]. The RMGIC absorption layer has been thought to act as s stress-breaking layer [49]. At the bottom of the absorption layer, hydroxyapatite that remained attached to individual collagen fibrils upon application of RMGIC (Vitrebond Plus) formed receptors for primary chemical bonding with polyalkenoic acids incorporated into the materials [16,50]. The deposition of this submicrom phase over the hybrid layer has been evidenced and can thus be regarded as a sub-layer of the earlier-documented absorption layer [23], identified as gel phase, gray intermediate or multilocular phase [16], which buffers the low pH [6].

The formation of strontium containing minerals is expected to occur in the presence of calcium and phosphate under high pH conditions [5]. Sr is normally added to substitute calcium due to its radiopaque properties, without affecting the setting products or cement's remineralizing capability [5], as Sr can be considered as an apatite-forming element [6]. Nevertheless, Sr has also been associated with caries prevalence [51], as its accumulation ceases in the region of the junction between demineralized zone and sound dentin [6]. Vitrebond Plus, in the unloaded group, made direct contact with apparently-hybridized dentin through the multilocular phase [10] without any sign of unprotected collagen at the interface (Fig. 5C). Nevertheless, a limited fringe of exposed proteins was detectable at Vitrebond Plus-interfaces when

load cycled was applied, more remarkable in CAD, especially at peritubular dentin. This sign evidenced a more advanced partial demineralization front (Fig. 5H). The loading stress which is concentrated mostly at the interface between the adhesive cement and the 2 μm thick hybrid layer [10] and within the hybrid layer [52, 53], may have accelerated the degradation of the resin-dentin interface, observed with the Masson's trichrome technique (Figs. 5D, 5H).

Ketac Bond applied on sound dentin showed 100% pretesting failures in both unloaded or load cycled samples (Fig. 1B). Taking into account that all pre-testing failures were considered as 0 MPa bond strength values during statistical analysis, there might be a sub-estimation of the mean MTBS of the GIC [13]. The surface of fracture showed a cohesive failure of the cement and displayed a particularly heterogeneous rough amorphous substance on top of dentin, and microscopic isolated spherical mineralized bodies scattered through the polyalkenoate matrix (Fig. 6A). Load cycling promoted the formation of rods-like mineralized connectors which maintained linked those spherical crystal precipitates (Fig. 6B). After load cycling, demineralized dentin collagen in CAD appeared completely remineralized in an extended net like-mineral below the typical gel-phase which represents the morphologic manifestation of a calcium-polycarboxylate salt (Fig. 7B). This salt resulted from reaction of the polyalkenoic acid with calcium extracted from dentin, and that was deposited on partially exposed dentinal collagen [17]. Additionally, dentinal tubules appeared mineral filled, almost hermetically sealed (Fig. 7B). Masson's trichrome staining technique revealed any sign of demineralization or exposed protein (red stain), *i.e.*, absence of unprotected collagen layer (Fig. 5F) was confirmed, matching with a substantial increase of mechanical properties (Hi and Ei) at the hybrid layer occurred in CAD when Ketac Bond was used and then load cycled (Fig. 3A).

Intrafibrillar mineralization is the key factor to ensuring that collagen fibrils have the same mechanical properties as occurs in natural biomineralized dentin [54]. Therefore, the increase of Hi and Ei of the partially demineralized collagen at the HL is directly related to the precipitation of minerals at the resin-dentin interface [55], and more specifically at the intrafibrillar compartment [1,54], leading to functional remineralization. Functional remineralization, therefore, is the result of a process that yields recovery of physical and chemical properties otherwise lost due to disease [56]. In this context, polyanionic molecules such as polyacrlylic acid allow the formation and stabilization of amorphous calcium phosphate. These nano-aggregates are thought to form flowable nano-precursors which can infiltrate the water filled gap zones in dentinal collagen fibrils, where they precipitate as polyelectrolyte-stabilized apatite nano-crystals [57]. This precipitation is guided by a polyphosphate molecule which acts as an apatite template, encouraging crystalline alignment, leading to hierarchical dentin remineralization [58]. Therefore, a functional remineralization effect, at the cement-dentin interface, can be inferred after using conventional GICs, i.e., Ketac Bond, in caries-affected dentin (Figs. 3A, 3B, 3C). Sound dentin did not show any potential site for functional remineralization, i.e., decreased intrafibrillar remineralization or lower mechanical properties (Fig. 2), attributed to the fact that the GIC requires preexistent nucleation sites, as in partially demineralize dentin (CAD). The diffusion of calcium/strontium ions into the hypomineralized matrix, accompanied by polyalkenoic acids will induce further demineralization, creating an ion-rich layer with mineral deposition on preexistent nuclei [59]. As a result, the local bioactivity of conventional GICs after in vitro load cycling can produce intrafibrillar mineralization at the interface, within the underlying dentin substrate. The advantage of this for the minimally invasive management of caries-affected dentin is self-evident.

19

In the present study, the increase in mechanical properties that produced the application of load cycling in CAD treated with Ketac Bond, at the HL, matched with bigger height of both phosphate (960 cm-[1]) (PO_4^{-3}, $v1$) and carbonate peaks (1070 cm-[1]) (CO_3^{2-}) (~1.97 and 1.27 fold, respectively), and so the area of phosphate (~1.32 fold) (Table 2A) (Fig. 4.IV·C). Four clusters were identified (Fig. 4.IV·B), corresponding to glass-ionomer cement (GIC), hybrid layer (HL), bottom of the hybrid layer (BHL) and dentin (DEN). The heights of the phosphate peaks followed the trend DEN > BHL > HL > GIC. The increment of the carbonate band refers a rise of carbonate substitution in the lattice structure of apatite [43], and coincides, after mechanical loading, with an increase (~1.30 fold) of the gradient of mineral content (GMC) [33] (Table 2A). The greater intensity of the red color at the scale (Fig. 4.IV·A), which corresponds to the intensity of the Raman scattered light of the phosphate peak corroborates this finding, in comparison to the unloaded specimen (Fig. 4.III·A). Nevertheless, the cement-dentin interfaces obtained with Ketac Bond applied on CAD specimens showed a decline of intensities in both phosphorous and calcium ions, as observed in the elemental analysis of the spectra (Figs. 7A-EDX and 7B-EDX). This lower intensities comes from the dissolution process which occurs after the conditioning step applied before the placement of the GIC [51]. On the other hand, Vitrebond Plus (RMGIC) applied on CAD substrata maintained higher relative intensities of P and Ca (Figs. 7C-EDX and 7D-EDX), as this restorative was applied without any previous conditioner. An increase of crystallinity in the mineral precipitates, *i.e.*, a decrease (~1.10 fold) of full width at half maximum (FWHM), respect to the unloaded specimens was shown in CAD specimens treated with Ketac Bond load cycled (Table 2A). FWHM expresses the crystallographic or relative atomic order, since narrower peaks suggest less structural

variation in bond distances and angles [33], and crystal strain [51]; in general, the narrower the spectral peak width is, the higher the degree of mineral crystallinity [34].

During mineralization, an important structural modification occurs in certain amino acid residues, as the generation of cross-links within their structure, which stabilizes the triple helix [45]. In line with those findings, a general movement toward higher frequencies of crosslinking [Pyridinium (1032 cm^{-1}), ratio 1031/1001 cm^{-1}, ratio phenyl/CH_2, and AGEs-pentosidine (1550 cm^{-1})] (Fig. 4.IV·C) was observable (Table 2B) after treatment of CAD surfaces with Ketac Bond load cycled [41]. Therefore, it can be assumed that improved crosslinking may contribute to increase both stability and mechanical properties at the dentin substrate [60], promoting nucleation [41]. The ratios which reflect the nature of collagen decreased, in general, at the interface after load cycling, confirming precarious recovery of organic components and worst collagen quality [43]. Peaks at 1340 cm^{-1} (α-helices) augmented (~1.03 fold), denoting a greater sensitivity to molecular orientation in order to enhance further crystallization [35] (Table 2C) (Fig. 4.IV·C). The spectral changes observed in the lipid bands (Table 2B) confirm the presence of tissue healing and maturation [45], as the height of peaks at 1440 and 1465 cm^{-1} increased ~1.15 and ~1.17 fold respectively in CAD treated with Ketac Bond mechanically loaded. Raman analysis also denoted a significant shift of the peak representing carboxyl group (COO^-) to a lower intensity when Ketac Bond was used on CAD, unloaded samples (Table 2B). This might suggest the formation and further increase of ionic bond with calcium [16], and match with an augment (~1.23 fold) of the peak at 1262 cm^{-1}, which reveals the presence of the ionomer acids and their salts [37, 59]. On the contrary, greater amount of carboxylic acid groups increases the available nucleation sites for mineralization because they can facilitate the binding with calcium ions, resulting in a faster mineral growth rate [61], as it occurred when Ketac

Bond was applied on CAD, and then load cycled (Table 2B), where 1415 cm^{-1} rose ~1.05 fold (Table 2B). The existence of an over-extended partial demineralization resulted associated to a previous demineralized dentin surface (CAD) which became further etched with the Ketac conditioner. Thereby, greater amount of ions may be expected at the interface. Furthermore, the presence of polycarboxylic acid is also augmented as it not only is part of the chemical composition of Ketac Bond, but it remained bound to dentin despite being rinsed off after conditioning [16]. The more intense and complete acid-base reaction which is expected to occur might have contributed to increase nucleation [61] and further mineralization.

Raman analysis of CAD treated with Vitrebond Plus load cycled convey a K-means clustering map quite different in comparison to Ketac Bond handled in similar conditions. Four independent clusters corresponding to glass-ionomer cement (GIC), hybrid layer (HL), bottom of the hybrid layer (BHL) and dentin (DEN), were also identified, but the distribution of the spectral variances associated for data differentiation changed between both groups. The chemical mapping resulted in a separated centroid-model in Ketac Bond (Fig. 4.IV·B) but less differentiated and scattered in Vitrebond Plus (Fig. 4.VIII·B). Application of Vitrebond Plus on CAD substrata originated new deposit of minerals whose height of phosphate and carbonate peaks augmented (~2.36 and 1.02 fold, respectively) after load cycling (Table 2A) (Figs. 4.VIII·A, 4.VIII·B), and so the crystallinity (lower FWHM) (~1.42 fold) (Table 2A). These findings concur with the relative intensity that was encountered between calcium and carbon elements (Figs. 7C-EDX, 7D-EDX), bigger than in the specimens treated with Ketac Bond (Figs. 7A-EDX, 7B-EDX), indicating a higher mineral content and a faster growth rate [61]. This advanced nucleation and further mineralization corresponded with lower collagen crosslinking at the interface than in the unloaded

22

samples, in general (Table 2B), as declined crosslinking of collagen usually results after nucleation [41]. Only AGEs-pentosidine (1550 cm^{-1}) augmented in this group (~1.37 in sound dentin, and ~1.09 fold in CAD, respectively). Tang and Vashishth, (2010) [62] have stated that an increase of AGE crosslink induces a marked decrease in the propagation fracture toughness, in bone. Indexes as mPPR (modified phosphate peaks ratio), *i.e.,* ratio between the mineral peak at 960 cm^{-1} (phosphate) (PO$_4^{3-}$) within the demineralized zone and the mineral peak (PO$_4^{3-}$) [36] within the caries affected substratum, and RMC (relative mineral concentration), *i.e.*, mineral-to-matrix ratio did also augment at the interface (~2.43 and 4.34 fold, respectively), after load cycling. Therefore, mechanical loading contributed to an increase of phosphate peaks and a decrease of peaks at phenyl group (1003 cm^{-1}) (Table 2B). The ratios which support the nature of collagen increased, in general, except in those where AGES-pentosidine became involved, (Table 2C), stating recovery, better organization, improved structural differences and collagen quality [41, 43,63]. On the contrary, a restricted collagen scaffolding was recorded after the decrease of both Amide I and III/AGEs-pentosidine ratios (Fig. 5IV.C). This fact gave rise to a delay in the advance of mineral precipitation [43], and resulted associate to a decrease in the intensity peak of α-helices (1340 cm^{-1}), worsening crystallization [35]. Height of lipid bands diminished at the interface after load cycling, denoting delayed dentin healing and maturation [45] (Table 2B). These findings comply with any improvement in both mechanical properties (Hi, Ei), at the cement-dentin interface (Fig. 3).

In sound dentin, load cycled specimens treated with Ketac Bond increased the relative mineral concentration (RMC) (~4.40 fold) (Table 2A) and originated extrafibrillar mineralization (Fig. 2A) with an increase of both phosphate (Figs. 4.IA, 4.IIA) and carbonate peaks at the interface (~5.08 and 2.26 fold, respectively) (Fig.

4.IIC). Those minerals resulted more crystalline (~1.50 fold) (Table 2A) than the unloaded samples. Indexes as PPR and GMC augmented and diminished, respectively (Table 2A), as results of the increase of phosphate peaks [36]. When Vitrebond Plus was used in sound dentin, load cycling application achieved a general opposite result, as both phosphate (Figs. 4.V·A, 4.VI·A) and carbonate peaks decreased at the interface (Fig. 4.VI·C) without any FWHM change (Table 2A), in junction with a decrease in the Young's modulus at the interface (Figs. 2C, 2D). Nevertheless, though the limited incorporation of Mg in apatite was shown to cause a reduction in crystallinity and increase in crystal strain [51], the slight detection of Mg in the elemental analysis (Fig. 6D-EDX) may not be significant, but it might increase the solubility and vulnerability of the apatite. Probably, the increase of the Raman peak after mechanical loading (~1.96 fold) (Table 2A) at 1262 cm^{-1} which corresponded to the chemical acids and their salts (Fig. 4.VI·C) might have hindered diffusion products and further crystallization [59]. In line with this chemical performance, PPR and GMC also fulfilled opposing outcomes to the conventional GIC (Ketac Bond).

A wide range of growth factors and matrix signaling molecules can be released or activated in dentin, remodeling and contributing to further tissue genesis and regeneration. These bioactive molecules become immobilized within the matrix, where they become fossilized in a protected stage thorough the interaction with other molecules and the mineral of the extracellular matrix [64]. It has been demonstrated that intermittent compressive load stimulates the proteic synthesis in osteoscytes and alkaline phosphatase activity in osteoblasts in vivo and in vitro. Alkaline phosphatase, present at all mineralization sites, hydrolyzes phosphate esters producing free phosphate, and thus apatite supersaturation [65]. On the other hand, reparative and reactionary dentin form in response to external stimuli, teeth injuries and dental caries.

24

Stimuli, injury and trauma can easily increase the pulpal hydrostatic pressure of the dentin structure. This pressure gradient (14–70 cm H_2O) from mechanical loading may increase interstitial fluid [66], fluid flow, which has been shown to have an important role in load-induced hard-tissue remodeling. This common occurrence can lead to some appropriate inductive molecular signals associated to an increase of calcified nodules and local amount of calcium, promotes calcium phosphate formation and stimulates matrix formation and mineralization [67]. Mechanical loading and fluid flow stimulate nitric oxide, which mediates signal transduction in hard tissues [66]. Flow-induced nitric oxide is biphasic, with a G-protein- and calcium-dependent burst associated with the onset of flow, and a G-protein- and calcium-independent phase associated with or steady sustained flow [68].

To the best of our knowledge, this is the first study aimed to evaluate the glass ionomer-dentin (sound and caries affected) interface by combining nano-mechanical, chemical and histological characterization. At present, further work is needed to provide a more detailed understanding of how and why Raman spectra of GICs-dentin interface vary with mechanical loading. This could be achieved by the use of this technique in junction with other methodologies, including FTIR. Also, effects of changes in temperature require more thorough investigation. Additional further investigations are also warranted to find out how the modifications observed correlate with temporal or spatial distribution of the healing or maturation processes in dentin remineralization events. Despite good potential, to undertake clinical studies are also recommended to confirm their bonding effectiveness as well as their better overall performance as restorative materials.

In summary, strengthened of the cement-dentin interface from remineralization, after mechanical loading, did not influence bond strength values, but produced the lowest percentage of adhesive failures in the present study. Morphologic analysis of surfaces displayed multiple mineral precipitates, deposited and integrated at the interface and within some tubules. Ketac Bond (conventional glass-ionomer cement) applied on sound dentin failed 100% cohesively. After load cycling, demineralized dentin collagen in CAD appeared completely remineralized, with total absence of unprotected collagen layer, below the typical gel-phase which represents the morphologic manifestation of a calcium-polycarboxylate salt. Maximal mechanical properties (Hi and Ei), at the hybrid layer, occurred in CAD when Ketac Bond was used and then load cycled, as result of functional remineralization after intrafibrillar remineralization. At the hybrid layer, samples with CAD treated with Ketac Bond and load cycled showed increase of both phosphate and carbonate groups, bigger gradient of mineral content and crystallinity which resulted in faster mineral growth rate. Those mineral changes were associated to increased crosslinking and worst collagen quality. Caries-affected dentin substrata treated with Vitrebond Plus (resin-modified glass-ionomer cement) and load cycled, showed an increase in the relative presence of minerals, relative mineral concentration and crystallinity, but lower collagen crosslinking associated to previous nucleation. The nature of collagen stated recovery, better organization, improved structural differences and collagen quality, but delay in the advance of mineral precipitation with worsening crystallization. These findings became associated to any changes in intrafibrillar mineralization, *i.e.,* mechanical performace improvement.

4. Conclusions.

At the hybrid layer, maximal functional or intrafibrillar remineralization occurred in caries-affected dentin surfaces when Ketac Bond was used and then load cycled, as a consequence of the highest values of both nanohardness and modulus of Young. This increase of nano-mechanical properties resulted associated to a complete absence of unprotected collagen, higher relative presence of minerals, crystallinity and crosslinking of collagen. Caries-affected dentin substrata did not attained any change in both nanohardness and modulus of Young when load cycling was applied on Vitrebond Plus, though minerals and crystallinity augmented, but crosslinking of collagen dropped.

At the hybrid layer of the interface achieved between both glass-ionomer cements and the caries-affected dentin, Ketac Bond showed higher nano-mechanical properties than Vitrebond Plus. In sound dentin, both cements performed similar, except in the load cycled group, where they obtained similar modulus of Young. At the bottom of the hybrid layer, load cycling promoted an increase in nonohardness when Ketac Bond was employed on caries-affected dentin. In sound dentin, nanohardness, at the bottom of the hybrid layer promoted after Ketac Bond infiltration, resulted higher than at interfaces obtained with Vitrebond Plus.

References

[1] Bertassoni LE, Habelitz S, Kinney JH, Marshall SJ, Marshall GW Jr. Biomechanical perspective on the remineralization of dentin. Caries Res 2009; 43:70-77.

[2] Wang Y, Spencer P, Walker MP. Chemical profile of adhesive/caries-affected dentin interfaces using Raman microspectroscopy. J Biomed Mater Res A 2007; 81: 279-286.

[3] Zheng L, Hilton JF, Habelitz S, Marshall SJ, Marshall GW. Dentin caries activity status related to hardness and elasticity. Eur J Oral Sci 2003;111: 243-52.

[4] Yoshiyama M, Tay FR, Torii Y, Nishitani Y, Doi J, Itou K, Ciucchi B, Pashley DH. Resin adhesion to carious dentin. Am J Dent 2003;16:47-52.

[5] Watson TF, Atmeh AR, Sajini S, Cook RJ, Festy F. Present and future of glass-ionomers and calcium-silicate cements as bioactive materials in dentistry: biophotonics-based interfacial analyses in health and disease. Dent Mater 2014; 30:50-61.

[6] Ngo HC, Mount G, Mc Intyre J, Tuisuva J, Von Doussa RJ. Chemical exchange between glass-ionomer restorations and residual carious dentine in permanent molars: an in vivo study. J Dent 2006; 34: 608-613.

[7] Baig MS, Fleming GJ. Conventional glass-ionomer materials: A review of the developments in glass powder, polyacid liquid and the strategies of reinforcement. J Dent 2015; doi:10.1016/j.jdent.2015.04.004.

[8] Yoshida Y, Van Meerbeek B, Nakayama Y, Snauwaert J, Hellemans L, Lambrechts P, Vanherle G, Wakasa K. Evidence of chemical bonding at biomaterial-hard tissue interfaces. J Dent Res 2000; 79:709-714.

[9] Shimada Y, Kondo Y, Inokoshi S, Tagami J, Antonucci JM. Demineralizing effect of dental cements on human dentin. Quintessence Int 1999; 30:267-273.

[10] Tay FR, Sidhu SK, Watson TF, Pashley DH. Water-dependent interfacial transition zone in resin-modified glass-ionomer cement/dentin interfaces. J Dent Res 2004; 83:644-649.

[11] Peumans M, Kanumilli P, De Munck J, Van Landuyt K, Lambrechts P, Van Meerbeek B. Clinical effectiveness of contemporary adhesives: a systematic review of current clinical trials. Dent Mater 2005; 21:864-881.

[12] Nakabayashi N, Pashley DH. Hybridization of Dental Hard Tissues. Tokyo: Quintessence Publishing Co, Ltd; 1998.

[13] Coutinho E, Cardoso MV, De Munck J, Neves AA, Van Landuyt KL, Poitevin A, Peumans M, Lambrechts P, Van Meerbeek B. Bonding effectiveness and interfacial characterization of a nano-filled resin-modified glass-ionomer. Dent Mater 2009;25:1347-1357.

[14] Chen L, Shen H, Suh BI. Bioactive dental restorative materials: a review. Am J Dent. 2013;26:219-227.

[15] Tanumiharja M, Burrow MF, Cimmino A, Tyas MJ. The evaluation of four conditioners for glass ionomer cements using field-emission scanning electron microscopy. J Dent 2001; 29:131-138.

[16] Coutinho E, Yoshida Y, Inoue S, Fukuda R, Snauwaert J, Nakayama Y, De Munck J, Lambrechts P, Suzuki K, Van Meerbeek B. Gel phase formation at resin-modified glass-ionomer/tooth interfaces. J Dent Res 2007; 86:656-661.

[17] Osorio R, Yamauti M, Osorio E, Román JS, Toledano M. Zinc-doped dentin adhesive for collagen protection at the hybrid layer. Eur J Oral Sci. 2011;119: 401-410.

[18] Wang Y, Spencer P. Hybridization efficiency of the adhesive/dentin interface with wet bonding. J Dent Res 2003;82:141-145.

[19] Li H, Burrow MF, Tyas MJ. The effect of load cycling on the nanoleakage of dentin bonding systems. Dent Mater 2002;18:111-119.

[20] de Mattos Pimenta Vidal C, Pavan S, Briso AL, Bedran-Russo AK. Effects of three restorative techniques in the bond strength and nanoleakage at gingival wall of Class II restorations subjected to simulated aging. Clin Oral Investig 2013;17:627-633.

[21] Toledano M, Cabello I, Aguilera FS, Osorio E, Osorio R. Effect of in vitro chewing and bruxism events on remineralization, at the resin-dentin interface. J Biomech 2015;48:14-21.

[22] Lynch RJ, Smith SR. Remineralization agents-new and effective or just marketing hype? Adv Dent Res. 2012;24:63-67.

[23] Sidhu SK, Watson TF. Interfacial characteristics of resin-modified glass-ionomer materials: a study on fluid permeability using confocal fluorescence microscopy. J Dent Res 1998;77:1749-1759.

[24] Koibuchi H, Yasuda N, Nakabayashi N. Bonding to dentin with a self-etching primer: the effect of smear layers. Dent Mater 2001;17:122-126.

[25] Toledano M, Aguilera FS, Sauro S, Cabello I, Osorio E, Osorio R. Load cycling enhances bioactivity at the resin-dentin interface. Dent Mater 2014;30:e169-e188.

[26] Sauro S, Osorio R, Watson TF, Toledano M. Therapeutic effects of novel resin bonding systems containing bioactive glasses on mineral-depleted areas within the bonded-dentine interface. J Mater Sci Mater Med 2012;23:1521-1532.

[27] Toledano M, Sauro S, Cabello I, Watson T, Osorio R. A Zn-doped etch-and-rinse adhesive may improve the mechanical properties and the integrity at the bonded-dentin interface. Dent Mater 2013; 29: e142-e152.

[28] Toledano M, Osorio E, Aguilera FS, Sauro S, Cabello I, Osorio R. In vitro mechanical stimulation promoted remineralization at the resin/dentin interface. J Mech Behav Biomed Mater 2014;30: 61-74.

[29] Almahdy A, Downey FC, Sauro S, Cook RJ, Sherriff M, Richards D, Watson TF, Banerjee A, Festy F. Microbiochemical analysis of carious dentine using Raman and fluorescence spectroscopy. Caries Res 2012;46:432-440.

[30] Nakabayashi N. The hybrid layer: a resin-dentin composite. Proc Finn Dent Soc 1992;88 (Suppl 1):321-329.

[31] Ager JW, Nalla RK, Breeden KL, Ritchie RO. Deep-ultraviolet Raman spectroscopy study of the effect of aging on human cortical bone. J Biomed Opt 2005;10: 034012.

[32] Toledano M, Aguilera FS, Osorio E, Cabello I, Toledano-Osorio M, Osorio R. Mechanical, chemical and morphological analysis of caries-affected dentin bonded with a Zn-doped resin. J Mech Behav Biomed Mater 2015 (Accepted for publication).

[33] Schwartz AG, Pasteris JD, Genin GM, Daulton TL, Thomopoulos S. Mineral distributions at the developing tendon enthesis. PLoS One 2012; 7: e48630.

[34] Karan K, Yao X, Xu C, Wang Y. Chemical profile of the dentin substrate in non-carious cervical lesions. Dent Mater 2009; 25: 1205-1212.

[35] Wang C, Wang Y, Huffman NT, Cui C, Yao X, Midura S, Midura RJ, Gorski JP. Confocal laser Raman microspectroscopy of biomineralization foci in UMR 106 osteoblastic cultures reveals temporally synchronized protein changes preceding and accompanying mineral crystal deposition. J Biol Chem 2009; 284: 7100-7113.

[36] Milly H, Festy F, Watson TF, Thompson I, Banerjee A. Enamel white spot lesions can remineralise using bio-active glass and polyacrylic acid-modified bio-active glass powders. J Dent 2014; 42:158-166.

[37] Young AM, Sherpa A, Pearson G, Schottlander B, Waters DN. Use of Raman spectroscopy in the characterisation of the acid-base reaction in glass-ionomer cements. Biomaterials 2000; 21:1971-1979.

[38] Xu C, Wang Y. Cross-linked demineralized dentin maintains its mechanical stability when challenged by bacterial collagenase. J Biomed Mater Res B Appl Biomater 2011; 96:242-248.

[39] Daood U, Iqbal K, Nitisusanta LI, Fawzy AS. Effect of chitosan/riboflavin modification on resin/dentin interface: spectroscopic and microscopic investigations. J Biomed Mater Res A 2013;101:1846-1856.

[40] Jastrzebska M, Wrzalik R, Kocot A, Zalewska-Rejdak J, Cwalina B. Raman spectroscopic study of glutaraldehyde-stabilized collagen and pericardium tissue. J Biomater Sci Polym Ed 2003;14:185-197.

[41] Xu C, Wang Y. Collagen cross linking increases its biodegradation resistance in wet dentin bonding. J Adhes Dent 2012;14:11-18.

[42] Sell DR, Monnier VM. Structure elucidation of a senescence cross-link from human extracellular matrix. Implication of pentoses in the aging process. J Biol Chem 1989; 264:21597-21602.

[43] Salehi H, Terrer E, Panayotov I, Levallois B, Jacquot B, Tassery H, Cuisinier F. Functional mapping of human sound and carious enamel and dentin with Raman spectroscopy. J Biophotonics 2013; 6:765-774.

[44] Strehle MA, Rösch P, Petry R, Hauck A, Thull R, Kiefer W, Popp J. A Raman spectroscopic study of the adsorption of fibronectin and fibrinogen on titanium dioxide nanoparticles. Phys Chem Chem Phys 2004; 6:5232-5236.

[45] Penel G, Delfosse C, Descamps M, Leroy G. Composition of bone and apatitic biomaterials as revealed by intravital Raman microspectroscopy. Bone 2005;36:893-901.

[46] Toledano M, Cabello I, Yamauti M, Osorio R. Differential resin-dentin bonds created after caries removal with polymer burs. Microsc Microanal 2012;18:497-508.

[47] Cheng HW, Lederer J, Cannel MB. Calcium sparks elementary events underlying excitation-contraction coupling in heart muscle. Science 1993;262:740-744.

[48] Watson TF, Bartlett DW. Adhesive systems: composites, dentine bonding agents and glass ionomers. Br Dent J 1994;176:227-231.

[49] Sidhu SK, Pilecki P, Cheng PC, Watson TF. The morphology and stability of resin-modified glass-ionomer adhesive at the dentin/resin-based composite interface. Am J Dent 2002;15:129-136.

[50] Yiu CK, Tay FR, King NM, Pashley DH, Sidhu SK, Neo JC, Toledano M, Wong SL.Interaction of glass-ionomer cements with moist dentin. J Dent Res 2004;83:283-289.

[51] LeGeros RZ. Chemical and crystallographic events in the caries process. J Dent Res 1990; 69 Spec No:567-574, discussion 634-636.

[52] Nikaido T, Kunzelmann KH, Chen H, Ogata M, Harada N, Yamaguchi S, Cox CF, Hickel R, Tagami J. Evaluation of thermal cycling and mechanical loading on bond strength of a self-etching primer system to dentin. Dent Mater 2002; 18: 269-275.

[53] Toledano M, Osorio R, Albaladejo A, Aguilera FS, Tay FR, Ferrari M. Effect of cyclic loading on the microtensile bond strengths of total-etch and self-etch adhesives. Oper Dent 2006; 31:25-32.

[54] Burwell AK, Thula-Mata T, Gower LB, Habelitz S, Kurylo M, Ho SP, Chien YC, Cheng J, Cheng NF, Gansky SA, Marshall SJ, Marshall GW. Functional

remineralization of dentin lesions using polymer-induced liquid-precursor process. PLoS One 2012;7:e38852. Erratum in: PLoS One. 2013;8(5).

[55] Balooch M, Habelitz S, Kinney JH, Marshall SJ, Marshall GW. Mechanical properties of mineralized collagen fibrils as influenced by demineralization. J Struct Biol 2008;162:404-410.

[56] Li Y, Thula TT, Jee S, Perkins SL, Aparicio C, Douglas EP, Gower LB. Biomimetic mineralization of woven bone-like nanocomposites: role of collagen cross-links. Biomacromolecules 2012;13:49-59.

[57] Tay FR, Pashley DH. Guided tissue remineralisation of partially demineralised human dentine. Biomaterials 2008;29:1127-1137.

[58] Liu Y, Kim YK, Dai L, Li N, Khan SO, Pashley DH, Tay FR. Hierarchical and non-hierarchical mineralisation of collagen. Biomaterials 2011;32:1291-1300.

[59] Atmeh AR, Chong EZ, Richard G, Festy F, Watson TF. Dentin-cement interfacial interaction: calcium silicates and polyalkenoates. J Dent Res 2012;91:454-459.

[60] Pugach MK, Strother J, Darling CL, Fried D, Gansky SA, Marshall SJ, Marshall GW. Dentin caries zones: mineral, structure, and properties. J Dent Res 2009; 88:71-76.

[61] Chen J, Chu B, Hsiao BS. Mineralization of hydroxyapatite in electrospun nanofibrous poly(L-lactic acid) scaffolds. J Biomed Mater Res A 2006;79:307-317.

[62] Tang SY, Vashishth D. Non-enzymatic glycation alters microdamage formation in human cancellous bone. Bone 2010;46:148-154.

[63] Toledano M, Aguilera FS, Cabello I, Osorio R. Remineralization of mechanical loaded resin-dentin interface: a transitional and synchronized multistep process. Biomech Model Mechanobiol 2014; 13:1289-1302.

[64] Smith AJ, Scheven BA, Takahashi Y, Ferracane JL, Shelton RM, Cooper PR. Dentine as a bioactive extracellular matrix. Arch Oral Biol 2012; 57:109-121.

[65] Posner AS, Blumenthal NC, Boskey AL. Model of aluminum-induced osteomalacia: inhibition of apatite formation and growth. Kidney Int 1986; 18: S17-S19.

[66] McAllister TN, Frangos JA. Steady and transient fluid shear stress stimulate NO release in osteoblasts through distinct biochemical pathways. J Bone Miner Res 1999; 14: 930-936.

[67] Li L, Zhu YQ, Jiang L, Peng W, Ritchie HH. Hypoxia promotes mineralization of human dental pulp   cells. J Endod 2011; 37: 799-802.

[68] Reijnders CM, van Essen HW, van Rens BT, van Beek JH, Ylstra B, Blankenstein MA, Lips P, Bravenboer N. Increased Expression of Matrix Extracellular Phosphoglycoprotein (MEPE) in Cortical Bone of the Rat Tibia after Mechanical Loading: Identification by Oligonucleotide Microarray. PLoS One 2013*;* 8: e79672.

Table 1 Materials and chemicals used in this study and respective manufacturers, basic formulation and mode of application

Product details	Basic formulation	Mode of application
Ketac Bond (3M Deustchland GmbH, Neuss, Germany)	*Powder:* calcium-aluminum-lanthanium-fluorosilica glass, pigments. *Liquid:* polycarboxylic acid, tartaric acid, water, conservation agents.	Apply Ketac conditioner [polycarboxylic (25% polyacrylic)acid] (10 s) Rinse with water. Mix powder and liquid components. Apply.
Vitrebond Plus (3M Deustchland GmbH, Neuss, Germany)	*Liquid:* resin-modified polyalkenoic acid, HEMA, water, initiators. *Paste:* HEMA, Bis-GMA, water, initiators and radiopaque FAS (BL7AL).	Mix paste/liquid components (10-15s). Apply. Light activation (20s).
X-FlowTM (Dentsply, Caulk, UK)	Strontium alumino sodium fluorophosphorsilicate glass, di- and multifunctional acrylate and methacrylate resins, DGDMA, highly dispersed silicon dioxide UV stabilizer, ethyl-4-dimethylaminobenzoate camphorquinone, BHT, iron pigments, titanium dioxide.	
SBFS (pH=7.45)	NaCl 8.035 g (Sigma Aldrich, St. Louis, MO, USA). NaHCO$_3$ 0.355 g (Sigma Aldrich, St. Louis, MO, USA). KCl 0.225 g (Panreac Química SA, Barcelona, Spain). K$_2$HPO$_4$·3H$_2$O 0.231 g, MgCl$_2$·6H$_2$O 0.311 g (Sigma Aldrich, St. Louis, MO, USA). 1.0 M – HCl 39 ml (Sigma Aldrich, St. Louis, MO, USA). CaCl$_2$ 0.292 g (Panreac Química SA, Barcelona, Spain). Na$_2$SO$_4$ 0.072 g (Panreac Química SA, Barcelona, Spain). Tris 6.118 g (Sigma Aldrich, St. Louis, MO, USA). 1.0 M – HCl 0–5 ml (Panreac Química SA, Barcelona, Spain).	

Abbreviations: HEMA: 2-hydroxyethyl methacrylate; Bis-GMA: bisphenol A diglycidyl methacrylate; FAS: fluoraluminosilicate; DGDMA: diethyleneglycol dimethacrylate phosphate; BHT: butylated hydroxytoluene; SBFS: simulated body fluid solution; NaCl: sodium chloride; NaHCO$_3$: sodium bicarbonate; KCl: potassium chloride; K$_2$HPO$_4$·3H$_2$O: potassium phosphate dibasic trihydrate; MgCl$_2$·6H$_2$O: magnesium chloride hexahydrate; HCl: hydrogen chloride; CaCl$_2$: Calcium chloride; Na$_2$SO$_4$: sodium sulfate; Tris: tris(hydroxylmethyl) aminomethane; SBFS: simulated body fluid solution; NaCl: sodium chloride; NaHCO$_3$: sodium bicarbonate; KCl: potassium chloride; K$_2$HPO$_4$·3H$_2$O: potassium phosphate dibasic trihydrate; MgCl$_2$·6H$_2$O: magnesium chloride hexahydrate; HCl: hydrogen chloride; CaCl$_2$: Calcium chloride; Na$_2$SO$_4$: sodium sulfate; Tris: tris(hydroxylmethyl) aminomethane.

Table 2A Mineral components in GIC-treated dentin surfaces

| | | | Relative Presence of Mineral | | | | FWHM | GMC Ratio C/P | PPR/healthy substratum | PAA & tartaric acids and their salts [1262] |
| | | | Phosphate [961] | | | Carbonate [1070] | | | | |
			Peak	Area	RMC	Peak	Phosphate			
Ketac Bond/ Sound dentin	Control	GIC	6.85	232.39	1.83	16.49	26.96	2.41	0.07	38.36
		HL	18.04	790.93	3.00	8.06	35.35	0.45	0.18	21.11
		BHL	19.28	549.73	7.11	7.22	22.51	0.37	0.19	17.00
		DEN	101.33	2492.88	19.30	18.07	19.33	0.18	1.00	20.23
	Load cycled	GIC	70.06	1720.7	11.77	14.36	19.28	0.20	0.69	18.63
		HL	81.29	1996.4	17.33	15.43	19.28	0.19	0.80	19.21
		BHL	108.48	2664.13	22.69	19.07	19.28	0.18	1.07	20.61
		DEN	126.2	3099.26	7.84	28.64	19.28	0.23	1.25	19.11
Ketac Bond/ Caries affected dentin	Control	GIC	12.62	647.59	2.31	12.43	41.81	0.98	0.08*	26.96
		HL	17.58	904.13	2.06	10.15	41.97	0.58	0.12*	19.19
		BHL	51.73	1275.04	9.56	12.31	25.83	0.24	0.35*	21.21
		DEN	67.66	2199.37	3.38	23.62	25.82	0.35	0.45*	31.66
	Load cycled	GIC	16.8	544.85	2.36	10.69	25.75	0.64	0.11*	19.17
		HL	28.19	926.58	4.03	12.08	41.97	0.43	0.19*	20.82
		BHL	104.61	2574.27	11.19	13.44	19.32	0.13	0.70*	21.03
		DEN	149.82	3686.89	11.41	21.38	19.32	0.14	1.00*	26.00
Vitrebond Plus/ Sound dentin	Control	GIC	12.03	436.13	2.10	10.34	28.94	0.86	0.09	27.27
		HL	22.95	564.59	2.72	10.88	19.30	0.47	0.18	22.66
		BHL	98.25	2025.34	14.06	19.51	16.08	0.20	0.76	22.56
		DEN	130.09	3199.97	12.43	24.13	19.30	0.19	1.00	26.04
	Load cycled	GIC	5.17	139.74	2.57	9.9	21.27	1.91	0.04	49.21
		HL	9.65	198.57	6.39	8.5	16.05	0.88	0.07	38.28
		BHL	37.91	930.17	35.10	10.34	19.27	0.27	0.29	50.53
		DEN	60.31	1479.92	27.79	11.18	19.27	0.19	0.46	23.04
Vitrebond Plus/ Caries affected dentin	Control	GIC	11.83	336.78	1.96	10.01	22.56	0.85	0.33*	18.36
		HL	12.35	492.03	2.30	9.22	32.23	0.75	0.35*	18.78
		BHL	13.16	374.87	2.19	10.17	22.56	0.77	0.37*	18.36
		DEN	17.66	642.47	3.44	8.03	29.22	0.45	0.49*	21.19
	Load cycled	GIC	22.94	564.49	8.69	8.31	19.32	0.36	0.64*	25.72
		HL	29.21	718.77	7.89	9.45	19.32	0.32	0.82*	23.95
		BHL	33.26	818.45	11.63	10.76	19.32	0.32	0.93*	21.59
		DEN	35.71	878.81	9.16	10.93	19.32	0.31	1.00*	22.24

Abbreviations: RMC: Relative Mineral Concentration between mineral/Phenyl (1003);
FWHM: Full-width half-maximum; GMC: Gradient in Mineral Content; PPR: Phosphate
Peaks Ratio; PAA: polyacrylic acid. Peaks positions are expressed in cm^{-1}.

*mPPR: modified Phosphate Peaks Ratio/ healthy substratum in caries affected dentin groups.

Table 2B Organics components in GIC-treated dentin surfaces (normalization, crosslinking, carboxilic group and lipids)

			Norma-lization	Crosslinking				Carboxilic group COO⁻	Lipids	
			Phenyl [1003]	Pyrid. [1032]	Ratio 1031/1001	Ratio phenyl/CH$_2$ [1003/CH]	AGEs-Pentosidine [1550]	[1415]	1440	1465
Ketac Bond/ Sound dentin	Control	GIC	3.74	5.17	1.38	0.26	18.9	11.01	13.35	13.59
		HL	6.01	1.56	0.26	0.34	19.47	11.96	23.60	25.53
		BHL	2.71	3.21	1.18	0.11	25.01	16.74	16.25	16.76
		DEN	5.25	6.91	1.32	0.29	9.66	10.90	15.56	15.93
	Load cycled	GIC	5.95	6.20	1.04	0.26	19.57	13.93	23.18	21.19
		HL	4.69	5.51	1.17	0.25	9.15	11.57	17.34	13.12
		BHL	4.78	7.22	1.51	0.24	10.62	11.0	18.31	15.10
		DEN	16.09	17.18	1.07	0.78	11.37	11.45	15.93	15.06
Ketac Bond/ Caries affected dentin	Control	GIC	7.10	4.92	0.69	0.27	23.74	25.49	26.46	22.97
		HL	4.59	4.01	0.87	0.20	26.87	18.64	20.19	20.41
		BHL	5.51	7.55	1.37	0.19	26.28	22.08	25.28	26.36
		DEN	9.86	10.35	1.05	0.42	17.33	17.3	20.41	20.66
	Load cycled	GIC	7.13	4.43	0.62	0.31	26.6	15.93	19.98	20.04
		HL	6.99	6.86	0.98	0.20	42.8	28.28	32.50	33.81
		BHL	9.35	8.58	0.92	0.40	18.26	14.43	19.70	20.88
		DEN	13.13	15.41	1.17	0.35	29.68	21.98	34.70	32.22
Vitrebond Plus/ Sound dentin	Control	GIC	5.72	4.52	0.79	0.27	17.43	13.26	18.66	18.98
		HL	8.44	5.09	0.60	0.54	14.73	7.91	14.03	14.21
		BHL	6.99	8.00	1.14	0.36	13.09	8.5	16.51	18.18
		DEN	10.47	9.10	0.87	0.44	12.51	9.8	9.52	19.28
	Load cycled	GIC	2.01	2.96	1.47	0.07	17.48	19.17	23.85	19.98
		HL	1.51	2.91	1.93	0.07	11.85	13.7	20.99	17.00
		BHL	1.08	1.38	1.28	0.02	26.26	35.29	43.14	38.42
		DEN	2.17	2.04	0.94	0.12	8.78	11.51	17.21	13.62
Vitrebond Plus/ Caries affected dentin	Control	GIC	6.04	8.79	1.46	0.35	13.69	4.3	12.79	17.01
		HL	5.38	8.21	1.53	0.31	9.8	5.91	14.04	17.28
		BHL	6.00	9.02	1.50	0.29	19.3	6.45	15.68	20.77
		DEN	5.13	5.12	1.00	0.30	12.31	4.43	11.35	16.29
	Load cycled	GIC	2.64	4.78	1.81	0.13	14.35	9.29	15.70	21.12
		HL	3.70	5.55	1.50	0.19	15.01	7.05	13.62	18.27
		BHL	2.86	6.64	2.32	0.16	16.84	4.42	11.87	17.97
		DEN	3.90	6.71	1.72	0.24	11.18	5.27	11.30	16.72

Abbreviations: A: Amide; Pyrid: Pyridinium; AGEs: Advanced glycation end products. Peaks positions are expressed in cm⁻¹.

Table 2C Organics components in GIC-treated dentin surfaces (Nature of collagen)

			Nature of collagen								
			A-III [1246-1270]	CH$_2$ [1450]	A-I [1655-1667]	Ratio Amide I/ Amide III	Ratio Amide III/ CH$_2$	Ratio Amide I/ CH$_2$	Ratio Amide III/ AGEs-Pentosidine	Ratio Amide I/ AGEs-Pentosidine	α-helices [1340]
Ketac Bond/ Sound dentin	Control	GIC	39.98	14.48	17.29	0.43	2.76	1.19	2.12	0.91	16.60
		HL	22.25	17.7	13.6	0.61	1.26	0.77	1.14	0.70	8.95
		BHL	17.35	25.53	12.93	0.75	0.68	0.51	0.69	0.52	14.95
		DEN	19.53	18.33	17.94	0.92	1.07	0.98	2.02	1.86	9.77
	Load cycled	GIC	18.27	23.18	24.39	1.33	0.79	1.05	0.93	1.25	8.46
		HL	19.05	18.58	15.10	0.79	1.03	0.81	2.08	1.65	9.08
		BHL	20.77	20.13	20.23	0.97	1.03	1.00	1.96	1.90	8.03
		DEN	20.21	20.73	20.04	0.99	0.97	0.97	1.78	1.76	6.79
Ketac Bond/ Caries affected dentin	Control	GIC	20.69	26.11	18.66	0.90	0.79	0.71	0.87	0.79	20.02
		HL	18.49	22.86	23.91	1.29	0.81	1.05	0.69	0.89	14.94
		BHL	24.85	28.90	36.42	1.47	0.86	1.26	0.95	1.39	19.19
		DEN	23.37	23.36	25.60	1.10	1.00	1.10	1.35	1.48	16.44
	Load cycled	GIC	19.04	23.33	20.49	1.08	0.82	0.88	0.72	0.77	15.53
		HL	19.55	35.73	29.38	1.50	0.55	0.82	0.46	0.69	20.06
		BHL	20.25	23.45	23.48	1.16	0.86	1.00	1.11	1.29	15.25
		DEN	28.90	37.02	35.28	1.22	0.78	0.95	0.97	1.19	24.79
Vitrebond Plus/ Sound dentin	Control	GIC	26.27	20.97	11.55	0.44	1.25	0.55	1.51	0.66	16.51
		HL	23.90	15.58	16.59	0.69	1.53	1.06	1.62	1.13	12.17
		BHL	23.01	19.45	22.02	0.96	1.18	1.13	1.76	1.68	14.20
		DEN	25.57	23.74	24.28	0.95	1.08	1.02	2.04	1.94	16.48
	Load cycled	GIC	50.75	26.91	14.26	0.28	1.89	0.53	2.90	0.82	18.94
		HL	39.93	22.39	10.82	0.27	1.78	0.48	3.37	0.91	15.11
		BHL	50.77	45.27	13.83	0.27	1.12	0.31	1.93	0.53	34.91
		DEN	23.44	18.25	12.84	0.55	1.28	0.70	2.67	1.46	12.70
Vitrebond Plus/ Caries affected dentin	Control	GIC	17.98	17.33	18.64	1.04	1.04	1.08	1.31	1.36	7.42
		HL	19.92	17.31	16.66	0.84	1.15	0.96	2.03	1.70	9.89
		BHL	17.60	20.98	24.42	1.39	0.84	1.16	0.91	1.27	8.62
		DEN	20.11	16.91	19.44	0.97	1.19	1.15	1.63	1.58	9.54
	Load cycled	GIC	23.18	21.07	17.87	0.77	1.10	0.85	1.62	1.25	12.37
		HL	20.99	19.01	18.98	0.90	1.10	1.00	1.40	1.26	10.34
		BHL	19.16	17.97	27.00	1.41	1.07	1.50	1.14	1.60	7.14
		DEN	19.83	16.44	19.10	0.96	1.21	1.16	1.77	1.71	8.38

Abbreviations: A-III: Amide III; A-I: Amide I. Peaks positions are expressed in cm^{-1}.

Figure captions

Fig.1 Mean microtensile bond strength (vertical lines are standard deviation) values (MPa) (A) and percentage distribution of failure mode (B) obtained for the different experimental groups. Differences were not encountered among groups

Fig.2 Mean and SD of nanohardness (Hi) (GPa) (A, B) and Young's modulus (Ei) (GPa) (C, D) measured at the experimental hybrid layers (HL) and bottom of hybrid layers (BHL) in sound dentin. Identical letters indicate no significant differences between unloaded restorations from the different experimental groups, identical numbers indicate no significant differences between load cycled restorations from the different experimental groups and * indicate significant differences between unloaded and load cycled restorations from the same experimental group

Fig.3 Mean and SD of nanohardness (Hi) (GPa) (A, B) and Young's modulus (Ei) (GPa) (C, D) measured at the experimental hybrid layers (HL) and bottom of hybrid layers (BHL) in caries-affected dentin. Identical letters indicate no significant differences between unloaded restorations from the different experimental groups, identical numbers indicate no significant differences between load cycled restorations from the different experimental groups and * indicate significant differences between unloaded and load cycled restorations from the same experimental group

Fig.4 Bi-dimensional (2D) micro-Raman map of the phosphate peak (961 cm^{-1}) intensities (A) and K-means clustering (KMC) map of the Raman profile of the same sample (B), in sound dentin unloaded (I,V), or load cycled (II,VI), or in caries-affected dentin unloaded (III,VII), or load cycled (IV,VIII). The color of the scale corresponds to the intensity of the Raman scattered light; red represents high intensity of phosphate peak and dark blue represents low intensity of phosphate peak. The plot is oriented such that the adhesive is in the lower aspect of the image and the dentin is in the upper

aspect. Raman *spectra* of principal components (PCs) is also observed (C): GIC, glass-ionomer cement; HL, hybrid layer; BHL, bottom of the hybrid layer; DEN, dentin

Fig.5 Representative light micrographs of Ketac Bond and Vitrebond Plus in sound and caries-affected dentin specimens; interfaces stained with Masson's trichrome: mineralized dentin stained green, adhesive stained beige, and exposed protein stained red. Original magnification: 150X. Ketac Bond control (unloaded) in sound (A), or caries-affected dentin (E). Ketac Bond load cycled in sound (B), or caries-affected dentin (F). Vitrebond Plus control (unloaded) in sound (C), or caries-affected dentin (G). Vitrebond Plus load cycled in sound (D), or caries-affected dentin (H). Demineralized dentin was not noticed at the bottom of the intermediate layer (arrows) (A). Light red or mild-orange stained areas were observed at Ketac Bond-dentin interface after load cycling in sound dentin (B); this staining was more pronounced at peritubular wall of caries-affected dentin (E) (arrow). Limited resin uncovered decalcified dentin was observed at Vitrebond Plus-sound dentin interface, unloaded (pointers) (C). Thinner evidence of partial demineralization or exposed protein, located at both intertubular (asterisk) and peritubular (arrow) dentin areas, may be detectable at Vitrebond Plus-sound dentin interface when load cycled (D). No signs of demineralization or exposed protein (red stain), *i.e.*, absence of unprotected collagen layer is detectable at Vitrebond Plus/dentin interface of specimens with caries-affected dentin unloaded (G) or Ketac Bond applied in caries affected dentin specimens and then load cycled (F). Vitrebond Plus/caries-affected dentin interface after load cycling (H) evidenced some partial demineralization and/or exposed protein (red stain), detectable as an increment in red intensity at both intertubular (pointer) and peritubular dentin (arrows)

Fig.6 Field-emission scanning electron microscopy images of failures after bonding and microtensile bond strength testing in sound dentin. (A) Ketac Bond unloaded. (B) Ketac Bond load cycled. (C) Vitrebond Plus unloaded. (D) Vitrebond Plus load cycled. (A) Unloaded specimens of Ketac Bond showed a cohesive failure in cement. Despite the presence of artifactual cracks in the polyalkenoate matrix (pointer), multiple spherical bodies (arrow) could be seen within the fractured glass-ionomer cement. The elemental analysis included phosphorous (P), calcium (Ca), and glass-filler components. (B) Specimens of sound dentin bonded with Ketac Bond, after load cycling is showing a cohesive failure of the cement. Interconnected spherical formations (pointer) were seen on the polyalkenoate matrix surface. Multiple rods-like bodies (arrows) linked those crystal precipitates. Espectrum from energy dispersive analysis, attained at zones 2a and 2b, is showing elemental composition of phosphorous (P) and calcium (Ca). (C) Unloaded specimens of sound dentin bonded with Vitrebond Plus showed a mixed failure at the top of the hybrid layer. Dentin (intertubular and peritubular) appeared porous and strongly mineralized. The precipitation of mineral formations only allowed a restricted display of the tubule entrances (arrow), deposited in progressive strata until the complete sealing of the lumen of tubule. The characteristic D-periodicity (67 nm) was revealed (pointers). Espectrum from energy dispersive analysis, attained at zone 3, is showing elemental composition of phosphorous (P) and calcium (Ca), as main components. (D) Specimens of sound dentin bonded with Vitrebond Plus, after load cycling, showed a mixed failure at the top of the hybrid layer. Intertubular dentin followed a mineralization pattern in clumps (arrows), while peritubular dentin appeared as strongly mineralized rings (asterisks) which permitted the visual observation of tubule walls. Mineralized collagen fibrils were noticeable in close contact with peritubular dentin (pointer). Special mineral formations, combination of both straight

rods and knob-like precipitates, were observed at the interface. Espectrum from energy dispersive analysis, attained at zone 4, is showing elemental composition of phosphorous (P) and calcium (Ca), as main components

Fig.7 Field-emission scanning electron microscopy images of failures after bonding and microtensile bond strength testing in caries-affected dentin. (A) Ketac Bond unloaded. (B) Ketac Bond load cycled. (C) Vitrebond Plus unloaded. (D) Vitrebond Plus load cycled. (A) Unloaded specimens of caries-affected dentin bonded with Ketac Bond showed a mixed failure at the top of the hybrid layer. A consistent and discontinuous layer of multiple clumps of precipitated minerals is observed covering the intertubular and peritubular dentin (asterisk), hiding the entrance of tubules. Espectrum from energy dispersive analysis, attained at zone 5, is showing elemental composition of phosphorous (P) and calcium (Ca), as main components, but with low intensity. (B) When Ketac Bond was used in specimens with caries-affected dentin and submitted to load cycling, an extended net like-mineral macro and microporous deposition was observed completely covering the dentin surface (left side of the image). Fractographic analysis discovered a crack representing cohesive failure in the cement, and the gel-phase remaining on top of dentin (right side of the image), with microscopic isolated particles of material (arrow) and deposits of mineral (pointer); as a result, dentin tubules were never directly exposed (asterisk). Some tubules appeared mineral filled, almost hermetically sealed (right top corner of the image); any collar of peritubular dentin was observable, and collagen fibrils resulted longitudinally mineralized, rounding the entrance of tubule (double arrow). Espectrum from energy dispersive analysis, attained at zone 6, is showing lower intensity of elemental components. (C) Unloaded specimens of caries-affected dentin bonded with Vitrebond Plus showed a mixed failure at the top of the hybrid layer. Strong mineralization of peritubular dentin was detectable. Growing

of mineral deposits at this location narrowed the lumen of tubule (arrow), or developed robust mineral cylinders within some other tubules (pointer). Multiple clumps of precipitated minerals appeared covering intertubular dentin (asterisk). Espectrum from energy dispersive analysis, attained at zone 7, is showing elemental composition of phosphorous (P) and calcium (Ca), as main components. (D) Specimens of caries-affected dentin bonded with Vitrebond Plus, after load cycling, showed a mixed failure at the top of the hybrid layer. Crystals precipitated in an extensive platform of mineral clumps, deposited on intertubular dentin (asterisk), at deeper areas of remineralization front. Interconnected knob-like formations were shown at superficial areas of this mineral front (arrow). Tubules appeared mineral free with a robust peritubular dentin wall (pointer). Espectrum from energy dispersive analysis, attained at zone 8, is showing the elemental composition of ions
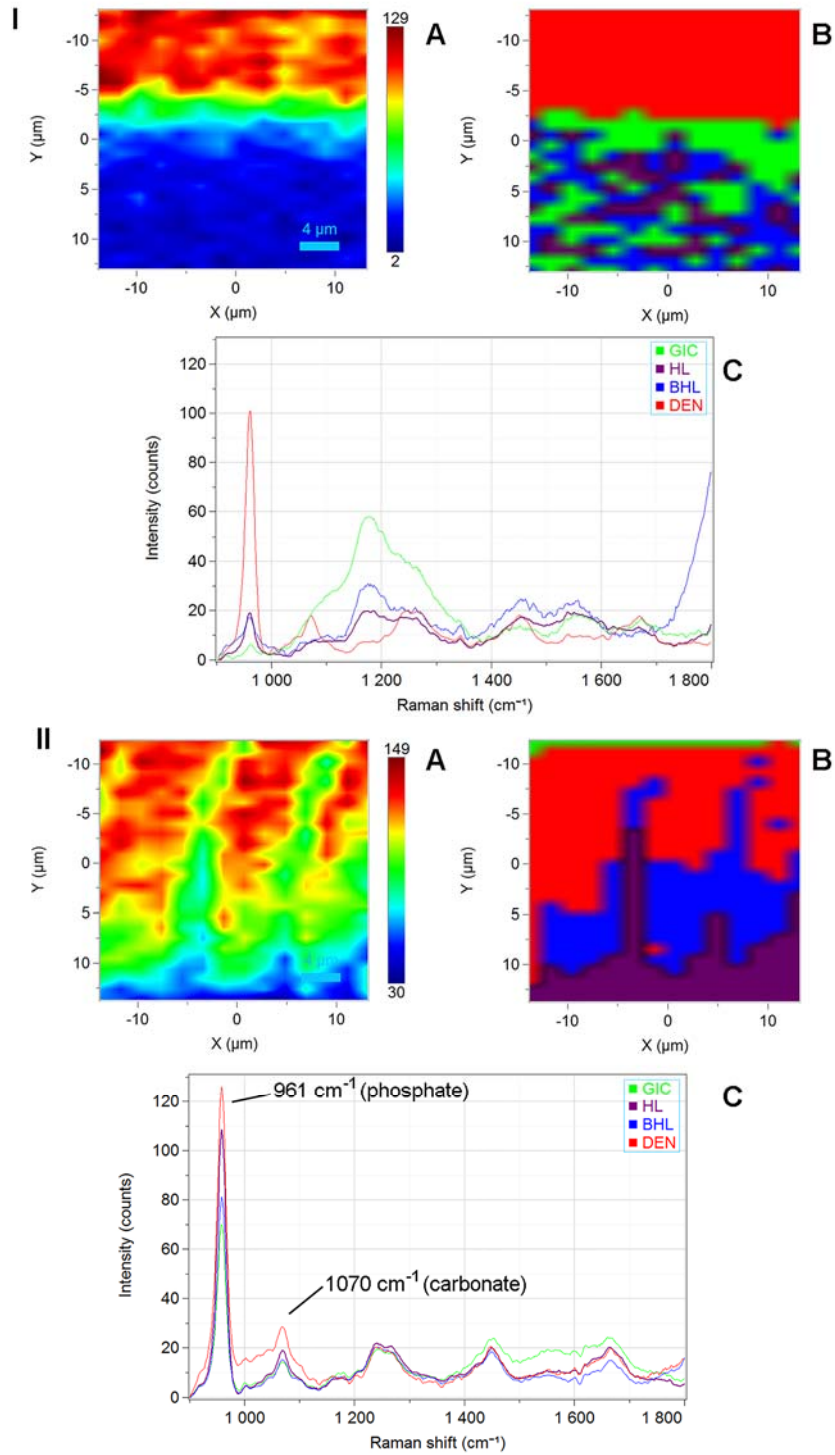
DIAGRAM 1
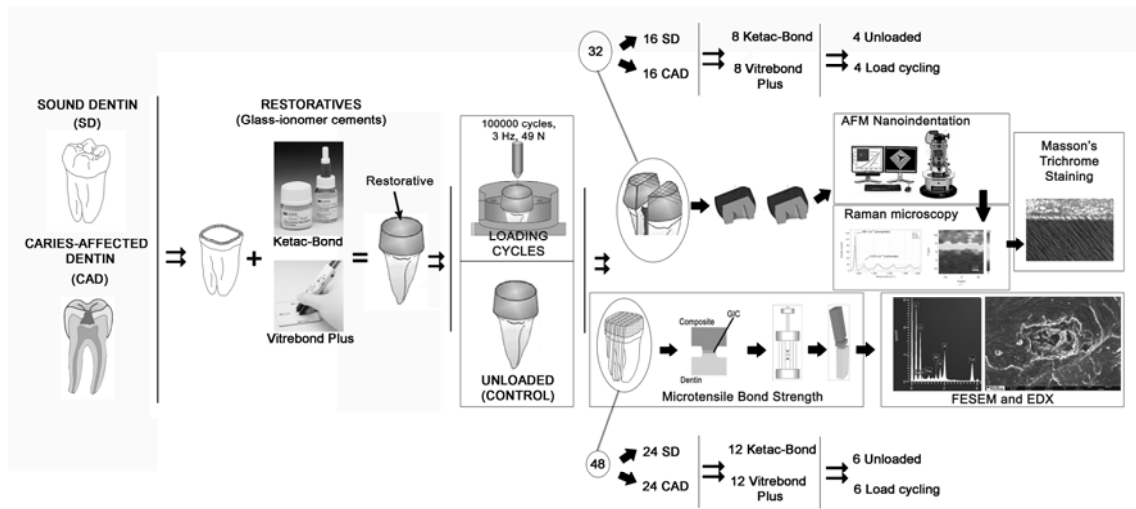
FIGURE 1

(A)
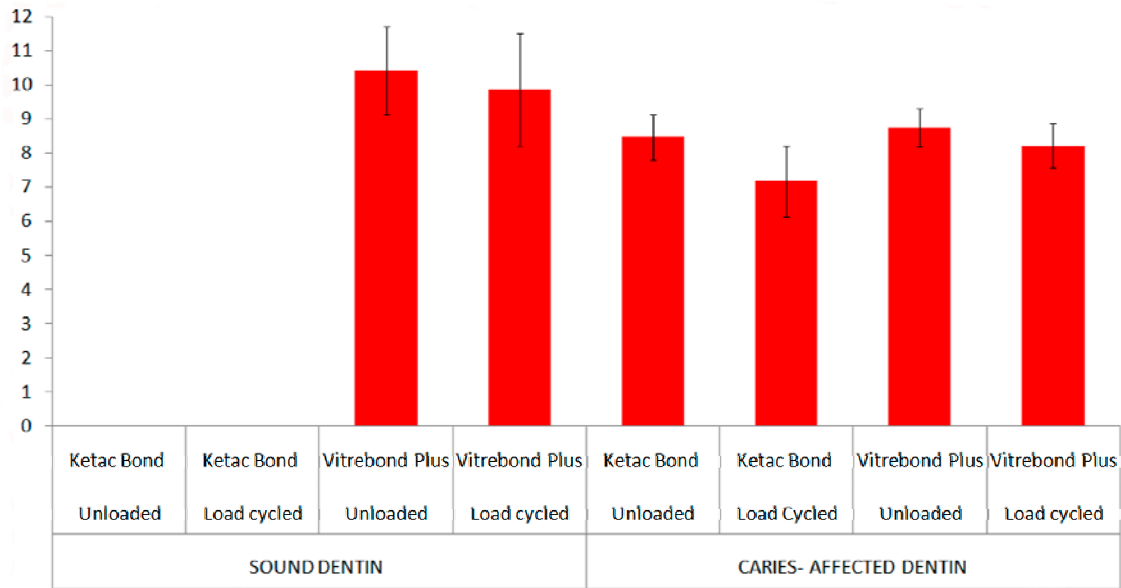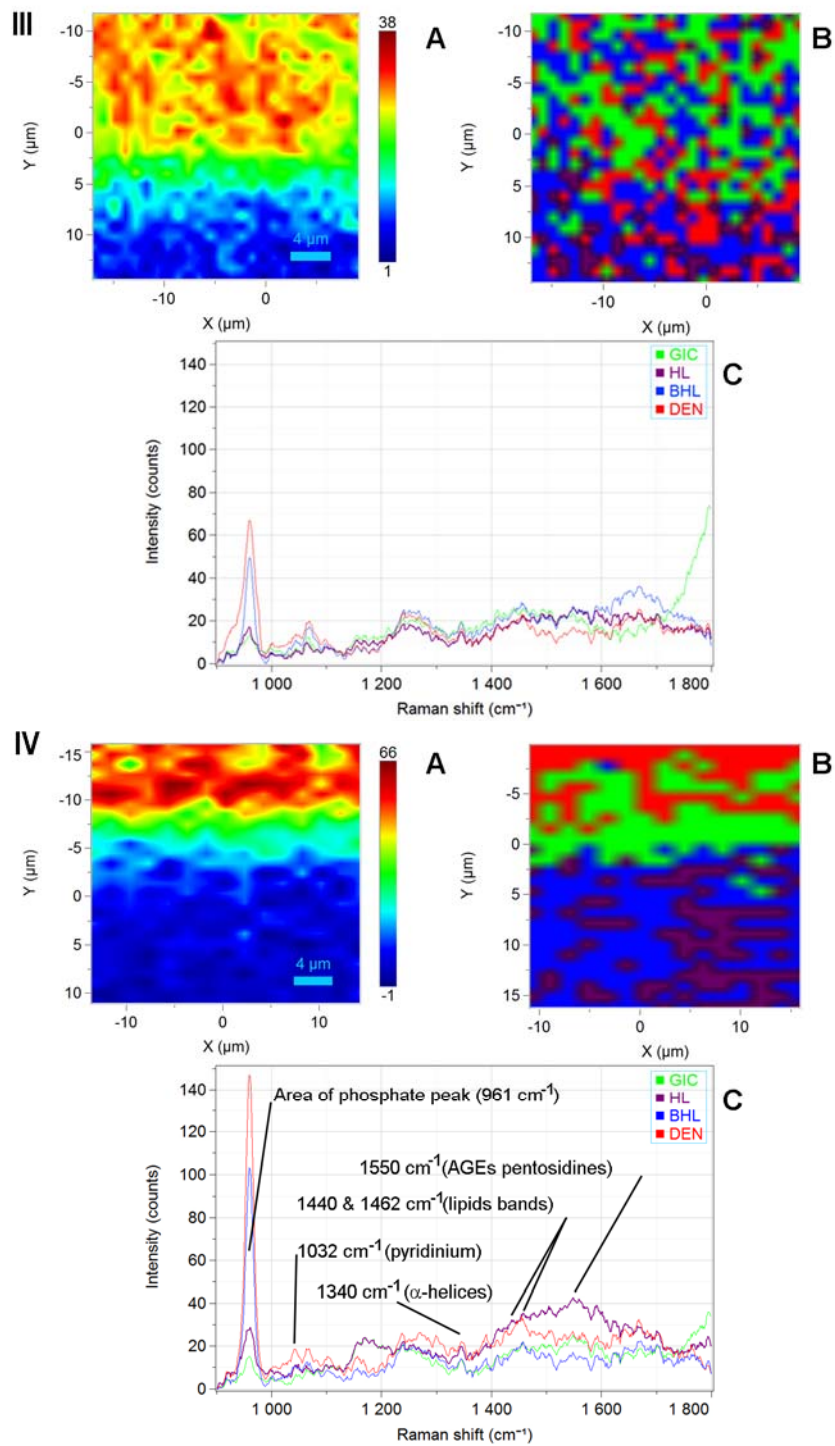

(B)
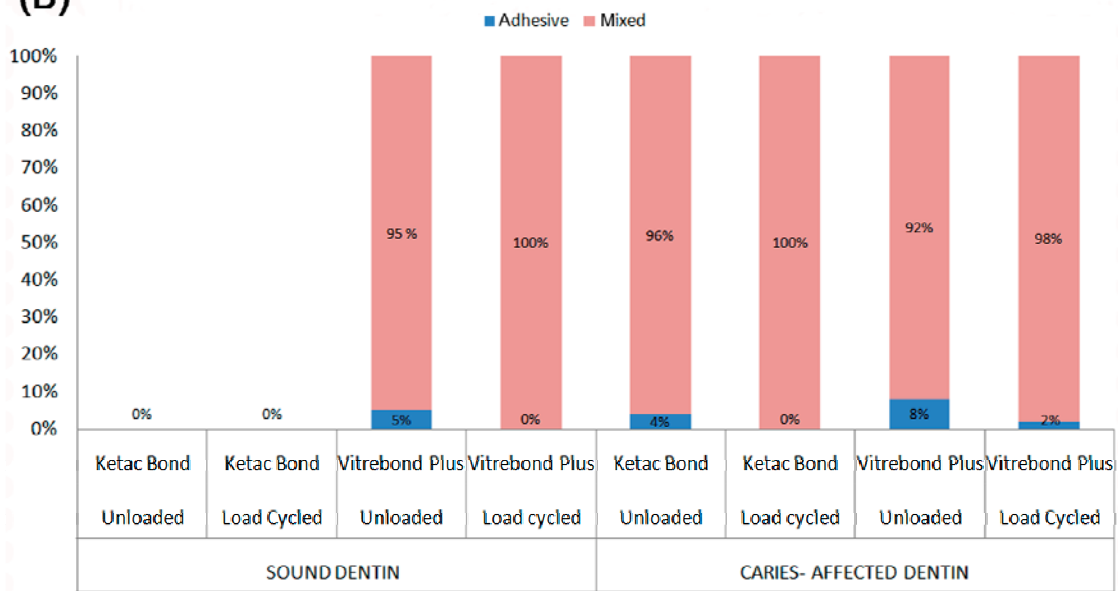
FIGURE 2
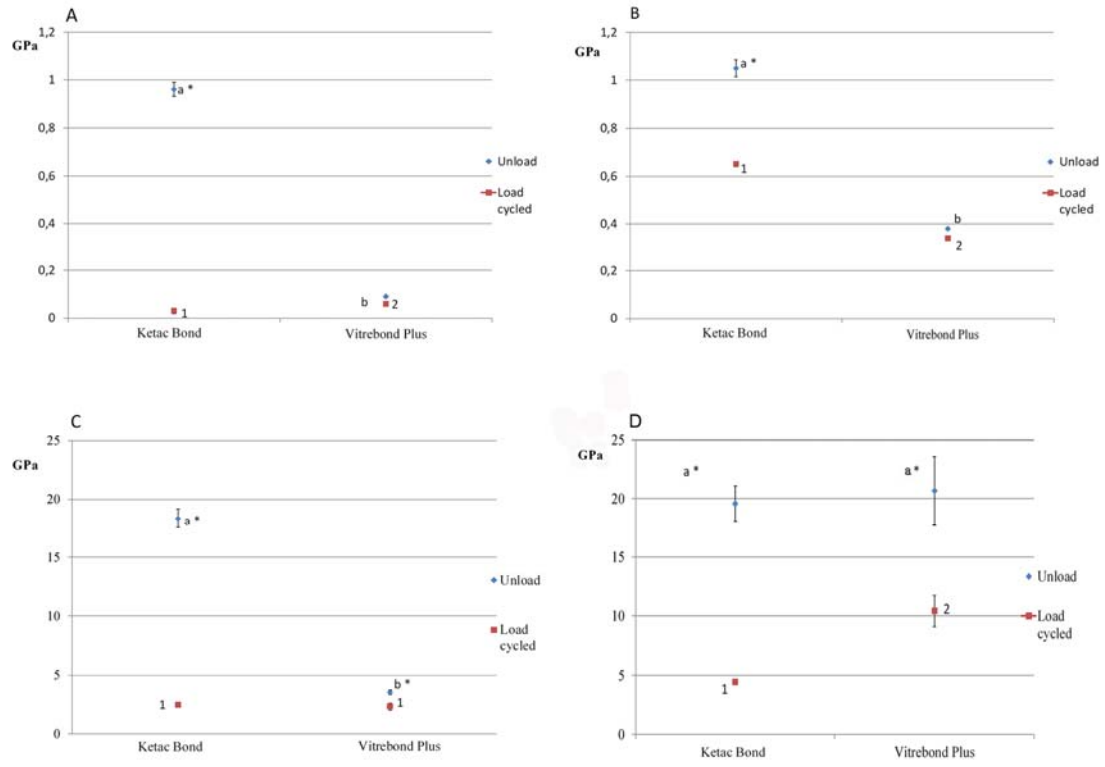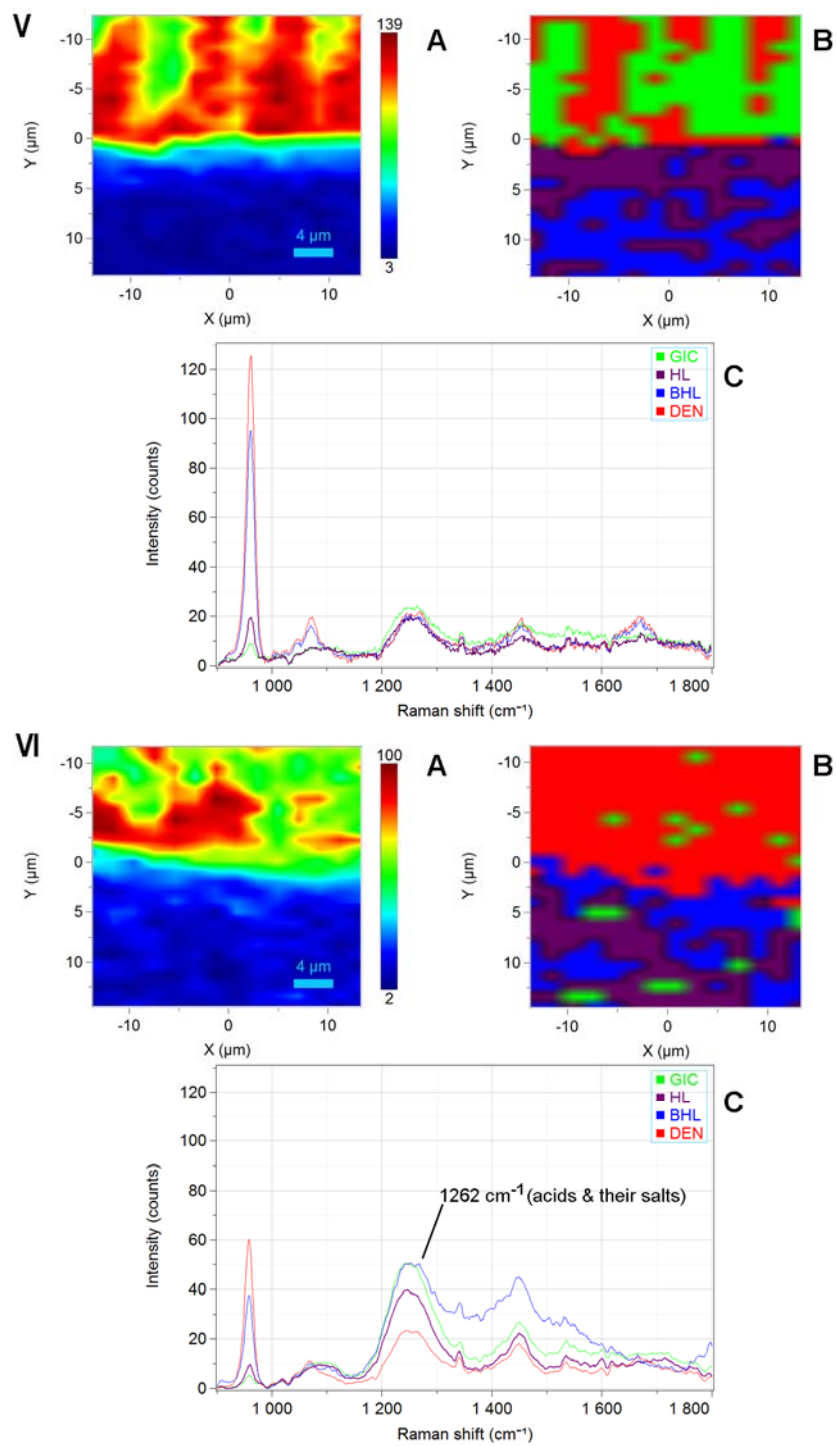
FIGURE 3
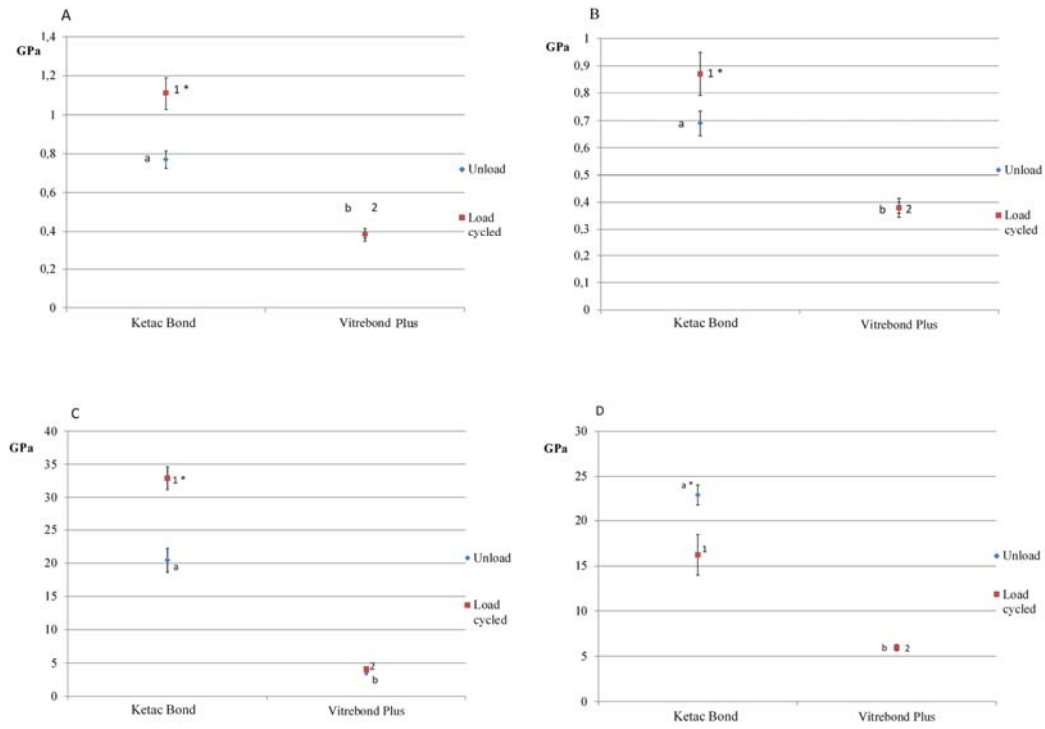
FIGURE 4 (I, II)
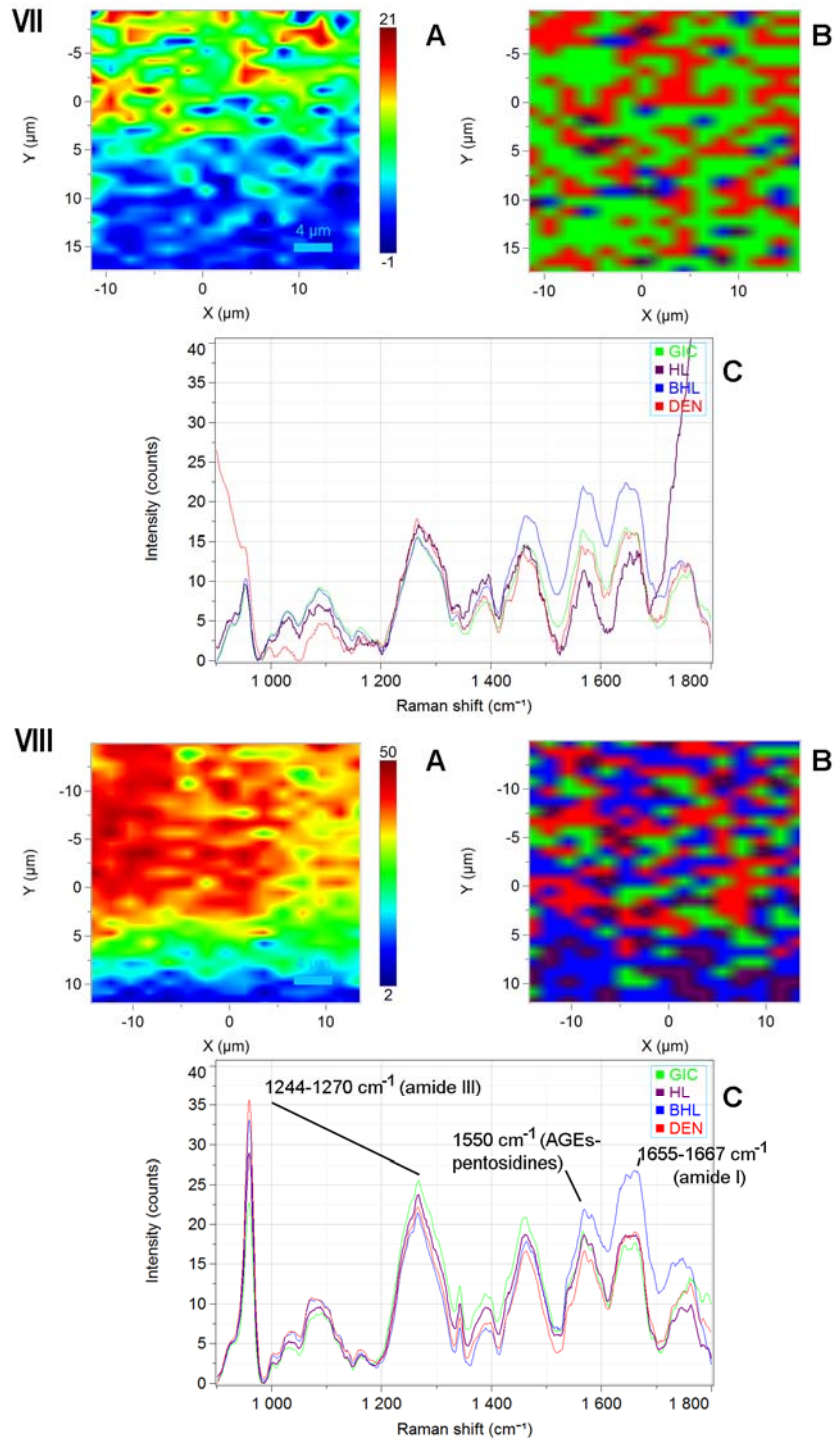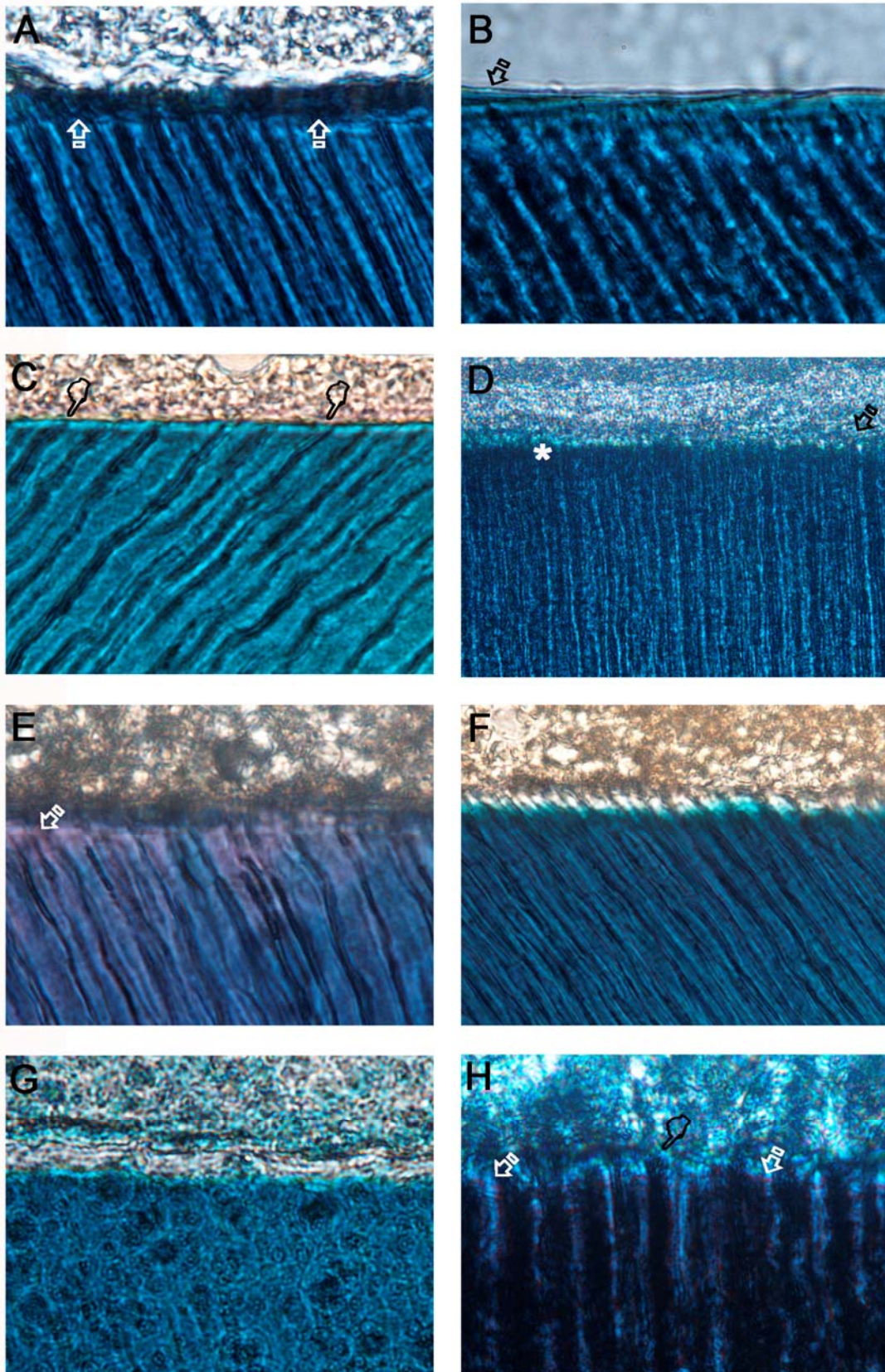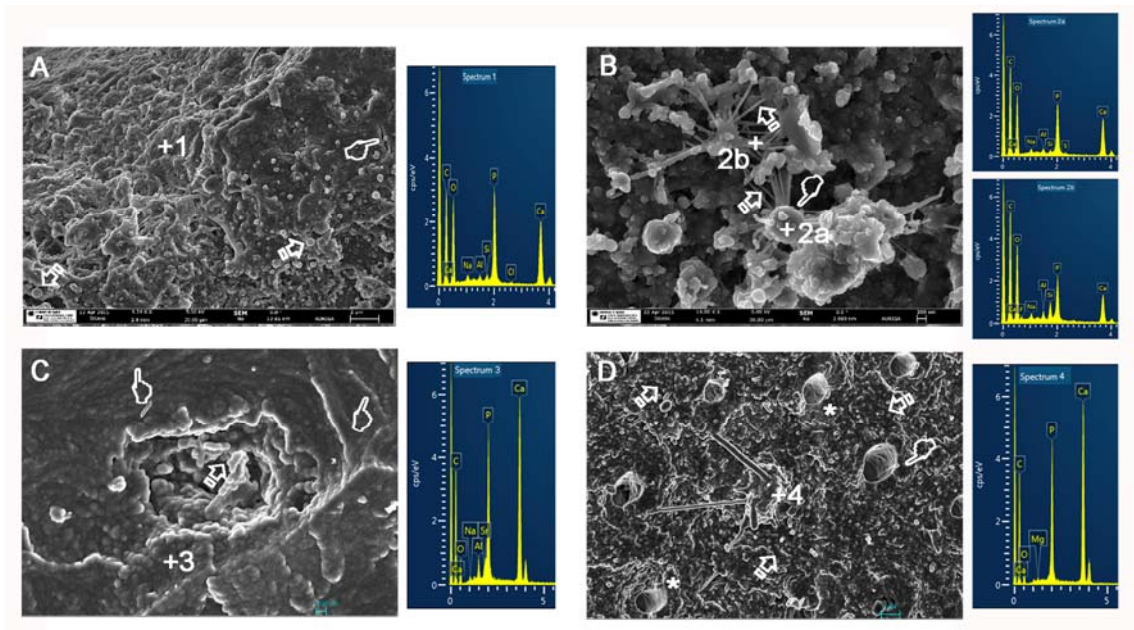
FIGURE 4 (III, IV)

FIGURE 4 (V,VI)

FIGURE 4 (VII, VIII)

FIGURE 5

FIGURE 6

FIGURE 7